Ruthenium-Platinum Polypyridyl Complexes: Synthesis and Characterization

R. Lee Williams Jr.

Thesis submitted to the Faculty of Virginia Polytechnic Institute and State University in partial fulfillment of the requirements for the degree of

Masters of Science
in
Chemistry

Karen J. Brewer, Ph.D., Chair
Paul A. Deck, Ph.D.
Brian M. Tissue, Ph.D.
Brenda S. J. Winkel, Ph.D.

August 21, 2001
Blacksburg, Virginia

Keywords. *polypyridyl, polyazine, ruthenium, platinum, bridging ligand, polymetallic,cisplatin, DNA*

Ruthenium-Platinum Polypyridyl Complexes: Synthesis and Characterization

R. Lee Williams

Abstract

A series of bimetallic (Ru^{II}, Pt^{II}) complexes were synthesized with the general formula $[(tpy)RuCl(BL)PtCl_2](PF_6)$ (tpy = 2,2′:6′,2″-terpyridine and BL = bridging ligand) and their spectroscopic, electrochemical, and DNA binding properties studied. The bridging ligands used in these complexes were 2,3-*bis*(2′-pyridyl)pyrazine (dpp), 2,3-*bis*(2′-pyridyl)quinoxaline (dpq) and 2,3-*bis*(2′-pyridyl)benzoquinoxaline (dpb). These complexes combine light-absorbing Ru^{II}-polypyridyl chromophores and a *cis*-$Pt^{II}Cl_2$ structural motif known to bind DNA. The Ru^{II}-bound chloride may be substituted, enabling further modification of the spectroscopic properties. The synthesis of $[(tpy)RuCl(BL)PtCl_2](PF_6)$ utilizes a building block approach that allows modifications to the series of complexes within the general synthetic scheme. This illustrates the applicability of this scheme to the development of new series of complexes.

The lowest-energy absorption for the three complexes is assigned to a $Ru(d\pi) \rightarrow BL(\pi^*)$ charge transfer transition. This transition shifts to lower energy as the ligand is varied from dpp to dpq to dpb. The first and second reductions are $BL^{0/-}$ and $BL^{-/2-}$ based and shift to more positive potentials from dpp to dpq to dpb. The $Ru^{II/III}$ redox couple remains at a nearly constant potential for the series. All three compounds show DNA binding

when incubated with linearized plasmid DNA. Adduct formation was assessed by agarose gel electrophoresis as a retardation of band migration.

Acknowledgements

With the completion of this thesis, I would like to offer my thanks to those who have made this accomplishment possible. I am indebted to many people who have offered their support and guidance including my family, friends, and the faculty and staff of Virginia Tech. In no way can I fully express my gratitude for the role they have played in shaping who I am.

I would first like to thank my parents, Ron and Debbie, who have always instilled in me and my sisters, Becky and Stacy, the strength of character to excel at whatever we take to task.

I would also like to thank my advisor Karen Brewer. Her support and criticism of this research project were instrumental to its success, as well as, my appreciation of the field.

Thanks go as well to Paul Deck, Brian Tissue, and Brenda Winkel for being interested instructors and scholars.

The Optical Sciences and Engineering Research Center, Carilion Biomedical Institute, and the National Science Foundation (CHE-9632713) have been generous in their financial support of this research.

Contents

List of Figures

List of Tables

List of Schemes

Abbreviations

BL	bridging ligand
bp	base pair
bpm	2,2′-bipyrimidine
bpy	2,2′-bipyridine
bpy^A-bpy^B	2,2′:3′,2″:6″,2‴-quaterpyridine
CT	charge transfer
dmso	dimethyl sulfoxide
DNA	deoxyribonucleic acid
dpb	2,3-*bis*(2-pyridyl)benzoquinoxaline
dpp	2,3-*bis*(2-pyridyl)pyrazine
dpq	2,3-*bis*(2-pyridyl)quinoxaline
ES	excited state
EtOH	ethanol
GS	ground state
HOMO	highest occupied molecular orbital
IL	intraligand
LA	light absorber
LF	ligand field
LMCT	ligand to metal charge transfer
LUMO	lowest unoccupied molecular orbital
mc	metal complex
MLCT	metal to ligand charge transfer
MO	molecular orbital
MW	molecular weight
MeBpy-Mebpy	4,4′-dimethyl-2,2′-bipyridine
PEt_2Ph	diethylphenylphosphine
4-Ph-py	4-phenylpyridine
pop	$P_2O_5H_2^{2-}$
PPh_3	triphenylphosphine
py	pyridine
RT	room temperature
tpp	2,3,5,6-tetrakis(2′-pyridyl)pyrazine
tpy	2,2′:6′,2″-terpyridine

CHAPTER 1: INTRODUCTION

Problem Statement

The goals of this research are to develop a building block synthetic strategy for a series of complexes, $[(tpy)RuCl(BL)PtCl_2]^+$ (tpy = 2,2′:6′,2″-terpyridine, and BL = bridging ligand), study the electrochemical and spectroscopic trends, and assess the metal complex-to-DNA binding affinity by agarose gel electrophoresis (Figure 1).

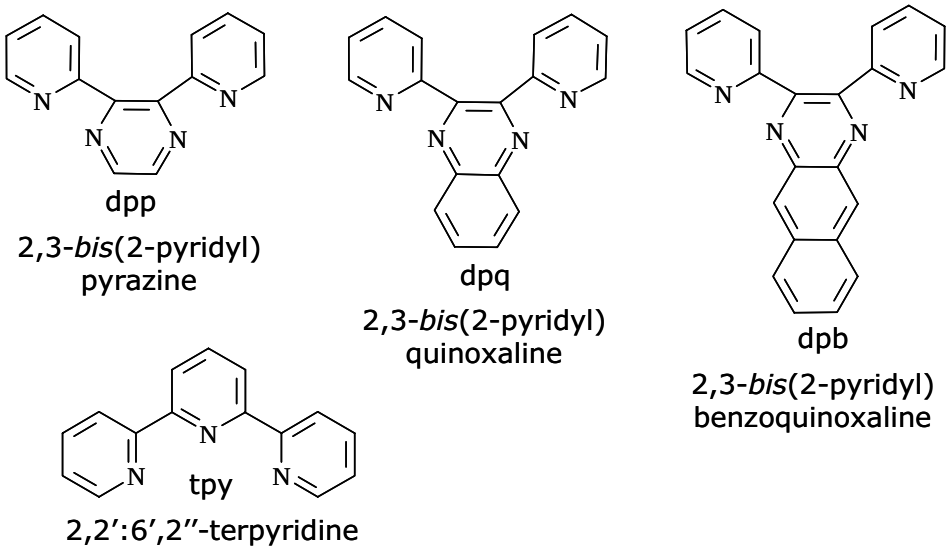

Figure 1. Bridging and terminal ligands used in the synthesis of $[(tpy)RuCl(BL)PtCl_2]^+$.

The series of complexes synthesized in this study combine the light-absorbing (LA) properties of Ru^{II} polypyridyl complexes and the DNA binding motif, *cis*-$PtCl_2$. The Ru and Pt metal atoms of the new bimetallic complexes are bridged by a series of *bis*-bidentate polyazine ligands; 2,3-*bis*(2-pyridyl)pyrazine (dpp), 2,3-*bis*(2-pyridyl)quinoxaline (dpq) and 2,3-*bis*(2-pyridyl)benzoquinoxaline (dpb). These ligands are similar in binding and structure. The difference in the degree of conjugation about pyrazine affects the electronic structure of the complex. The BLs introduce systematic

variation of the electronic structure without significantly altering the metal coordination. Because these changes are systematic, comparisons within the series aid in making assignments to the rich but complicated spectroscopic and electrochemical properties. The use of a tridentate terminal ligand leaves an easily-substituted chloride ligand on ruthenium. The electronic properties of the complex can be tuned by future substitution of the chloride. The synthetic strategy, electrochemical and spectroscopic trends, and DNA binding affinity of these $[(tpy)RuCl(BL)PtCl_2]^+$ complexes are discussed in the next two sections of this thesis.

Ruthenium-Polypyridyl Complexes

The interest in Ru-polypyridyl complexes began with the initial discovery of $[Ru(bpy)_3]^{2+}$.[1] Photoinduced excited-state properties of this complex led researchers to study a wide array of Ru^{II}-polypyridyl complexes. A combination of photochemical and photophysical properties has led to the design of complexes that are useful for solar energy conversion schemes,[2] photosynthetic mimics,[3] bimolecular probes[4] and other applications.[5]

Localized Molecular Orbital Description. Polyazine ligands possess a filled highest occupied molecular orbital (HOMO) and a vacant lowest unoccupied molecular orbital (LUMO) of the appropriate energy to interact with metal d-orbitals. Upon coordination, the polyazine ligands donate electron density from nitrogen sp^2 hybridized orbitals (lone pairs) to metal p and s orbitals to form a σ-bond. The electron-rich metal ion transfers electron density back from it's d orbitals to the π^* orbitals of the polyazine aromatic ligand to form a weak π bonding interaction. The synergistic interaction stabilizes the low oxidation state of Ru^{II} and gives rise to the unique spectroscopic and electrochemical properties of Ru-polypyridyl complexes.

The spectroscopic and electrochemical properties of Ru^{II} polypyridyl complexes are described in terms of a localized molecular orbital (MO) approximation (Figure 2).[6] For example, the MO formed by the combination of the nitrogen lone pair of electrons on a ligand and metal orbitals is labeled σ_L since it receives the greatest contribution from the ligand orbital and retains mostly ligand character.

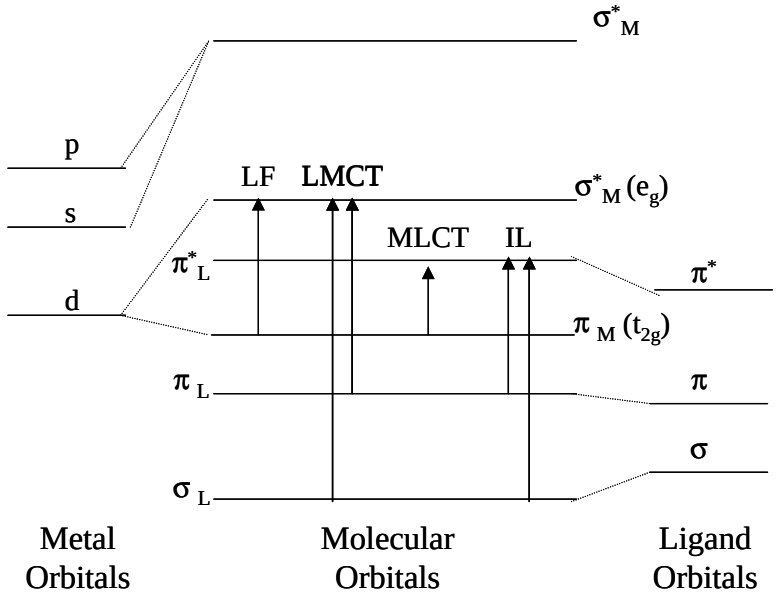

Figure 2. Molecular orbital diagram for an octahedral transition metal complex.

For Ru^{II} polypyridyl complexes, the σ_L and π_M MOs are filled while σ^*_M, π^*_L and higher MOs are empty. Excitation with light redistributes the orbital population and is described by a single excited-state MO configuration. The various spectral transitions are summarized in Figure 3. Ligand field transitions (LF) occur between MOs that are predominantly metal-based while intraligand (IL) transitions occur between MOs that are predominantly ligand-based ($n \rightarrow \pi^*$ and $\pi \rightarrow \pi^*$). Charge transfer (CT) transitions involve the redistribution of electron density between the metal and ligand MOs. The transitions occur as metal-to-ligand CT (MLCT) and ligand-to-metal CT (LMCT) depending on the energies of the MOs involved.[6]

Electrochemical processes are also described in terms of the localized MO approximation. Oxidations are usually metal-based and indicate the energy of the highest occupied MO (HOMO). Reductions are typically ligand-based, although there are some examples in which a metal undergoes a reduction within the solvent window.[7] The first reduction process correlates with the energy of the lowest unoccupied MO (LUMO). Because the added electrons of a reduction process are typically isolated in the π^* network of a single ligand, complexes are stable through several reductions.[8]

Spectroscopic and Electrochemical Properties. The prototypical complex, $[Ru(bpy)_3]^{2+}$, exhibits an intense $Ru(d\pi)\rightarrow bpy(\pi^*)$ (MLCT) absorption band in the visible spectrum (450 nm in acetonitrile) (Figure 3).[9] The excited-state emits strongly at 630 nm in deoxygenated acetonitrile with a long excited-state lifetime of 600 ns at room temperature.[9]

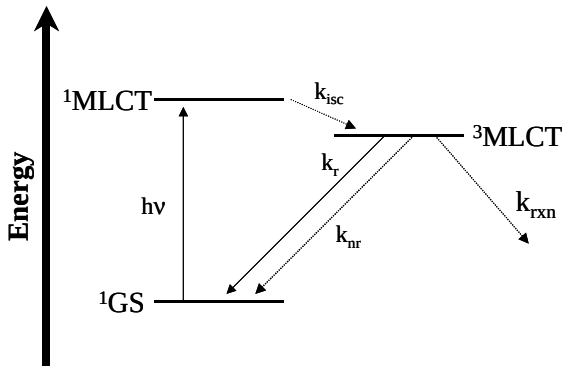

Figure 3. Jablonski diagram of $[Ru(bpy)_3]^{2+}$.

Characterization of the excited-state as a MLCT can be thought of as an intramolecular redox process in which Ru undergoes a formal one-electron oxidation and bpy undergoes a formal one-electron reduction. When excited, an electron moves from an orbital that is predominately Ru-based to an orbital that is predominately ligand-based. This redistribution of electron density leaves a complex that is both a more powerful oxidizing and

reducing agent than the ground state and able to undergo oxidative and reductive electron transfer quenching. The excited-state is also deactivated by energy transfer. An important example is the deactivation of ^{3}MLCT excited-state by ground state triplet oxygen.[5] Oxygen in a highly reactive excited singlet state causes oxidative damage to DNA and other analytes.[5] One difficulty in harnessing the energy trapped in the ES for chemical processes is that energy or electron transfer to a quencher depends on collisional contact during the excited-state lifetime. Additionally, back electron transfer limits the efficiency these processes.

The electrochemical characteristics of $[Ru(bpy)_3]^{2+}$ are also interesting. The $Ru^{II/III}$ one-electron oxidation leaves the complex in a low spin $(t_{2g})^5$ configuration that is inert to ligand substitution. Reductions are localized on the bpy ligands leaving Ru in an inert, low spin $(t_{2g})^6$ configuration.[10] In DMF at −54 °C, six reversible bpy-based redox processes are observed.[11]

Tuning Spectroscopic and Electrochemical Properties. The GS and ES properties of Ru^{II} polypyridyl complexes can be modified with the selection of ligands having different σ-donating and π-accepting abilities. For example, the tridentate ligand, tpy, has been investigated as an analogue of bpy in ruthenium complexes. The similarities in the structure and coordination of these ligands leads to the expectation that Ru complexes constructed with either ligand would have similar spectroscopic features (Figure 4). In fact, $[Ru(tpy)_2]^{2+}$ exhibits an intense Ru (dπ) → tpy (π*) CT absorption centered at 476 nm, slightly red shifted from the $[Ru(bpy)_3]^{2+}$ MLCT.[12] The *bis*-tpy complex does not, however display an easily-detectable emission at room temperature (RT) and has a short ES lifetime (250 ps).[12] The unfavorable bite angle stain associated with the tpy ligand results in a weakened ligand field in $[Ru(tpy)_2]^{2+}$ and a lower energy ^{3}LF (ligand field)

state. The thermally-accessible LF state undergoes rapid, non-radiative deactivation to the ground state and quenches the luminescent ^{3}MLCT state. The short-lived excited-state of $[Ru(tpy)_2]^{2+}$ has limited the study of tpy-based chromophores.

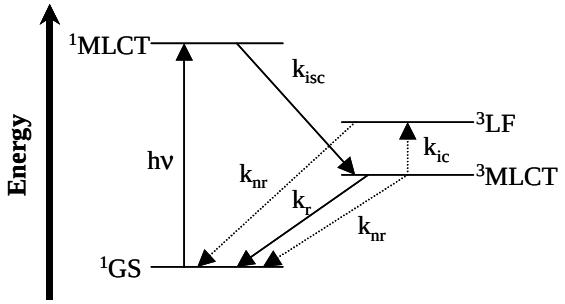

Figure 4. Jablonski diagram of $[Ru(tpy)_2]^{2+}$.

The introduction of the *bis*-tridentate ligand tpp (tpp = 2,3,5,6-*tetrakis*(2-pyridyl)pyrazine) gives rise to a long ES lifetime in the complex $[(tpy)Ru(tpp)]^{2+}$ (Figure 5). Tpp is similar to tpy with the addition of two

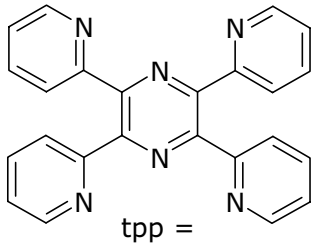

2,3,5,6-tetrakis(2'-pyridyl)pyrazine

Figure 5. *bis*-Tridentate bridging ligand tpp.

pyridyl groups (py) and a central pyrazine. The lower energy of the tpp-based π^* orbitals lowers the energy of the LUMO in $[(tpy)Ru(tpp)]^{2+}$ (Figure 6). The resulting tpp-based lower-lying MLCT state has an absorption maximum at 472 nm and is a Ru (dπ) → tpp (π^*) CT transition.[12] The complex has a RT emission centered at 684 nm with an ES lifetime of 91 ns.

The intense emission and longer lifetime are attributed to a low -lying ^{3}MLCT that limits the thermal population of the higher energy ^{3}LF state.

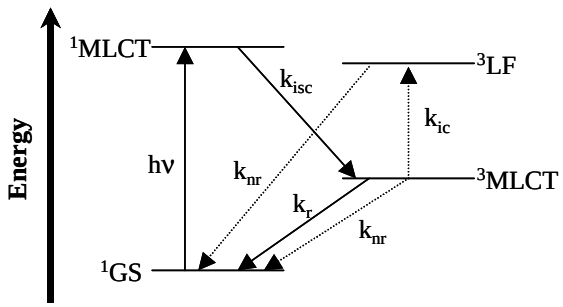

Figure 6. Jablonski diagram of $[(tpy)Ru(tpp)]^{2+}$.

A series of tpy-containing complexes, $[(tpy)RuCl(BL)]^+$ and $[(tpy)Ru(py)(BL)]^{2+}$ (py = pyridine and BL = dpp, dpq, and dpb), have been studied.[13] The *bis*-bidentate ligands used in these complexes differ in the number of rings fused to pyrazine. The stepwise increase in conjugation stabilizes the π^* acceptor orbitals with each additional ring and is confirmed by the positive shift in reduction potentials of the free ligands (Table 1).[14] The trend is maintained upon coordination to Ru, and results in a

Table 1. Reduction potentials for dpp, dpq, and dpb.[14]

Ligand	$E_{½}$ [a] (V)
dpp	-1.80
dpq	-1.43
dpb	-1.14

[b]Potentials reported vs. Ag/AgCl (0.286 vs. NHE) in CH_3CN solution with 0.1 M Bu_4NPF_6.

progressively lower Ru (dπ) → BL (π^*) CT absorption through the series dpp to dpq to dpb (Table 2). The pyridine complexes are also emissive at RT with an ES lifetime of 80 ns for the species bridged by dpp.

Table 2. Electronic absorption data for $[(tpy)RuCl(BL)]^+$ and $[(tpy)Ru(py)(BL)]^{2+}$ where py=pyridine, tpy = 2,2′:6′,2″-terpyridine, and BL = 2,3-*bis*(2′-pyridyl)pyrazine (dpp), 2,3-*bis*(2′-pyridyl)quinoxaline (dpq) and 2,3-*bis*(2′-pyridyl)benzoquinoxaline (dpb).[13]

	λ_{max}^{abs} (nm)[a]	$E_{½}$ (V)[b]	
		$Ru^{II/III}$	$BL^{0/-}$
$[(tpy)RuCl(dpp)]^+$	510	+1.04	-1.07
$[(tpy)RuCl(dpq)]^+$	570	+1.06	-0.77
$[(tpy)RuCl(dpb)]^+$	595	+1.02	-0.61
$[(tpy)Ru(py)(dpp)]^{2+}$	475	+1.42	-1.04
$[(tpy)Ru(py)(dpq)]^{2+}$	520	+1.41	-0.75
$[(tpy)Ru(py)(dpb)]^{2+}$	555	+1.44	-0.59

[a]Reported for the lowest-lying transition. Recorded in CH_3CN.
[b]Potentials reported vs. Ag/AgCl (0.286 V vs. SHE) in CH_3CN solution with 0.1 M Bu_4NPF_6.

Both of these complexes, $[(tpy)RuCl(BL)]^+$ and $[(tpy)Ru(py)(BL)]^{2+}$, have a bidentate and tridentate ligand, leaving Ru with a labile ligand in the coordination sphere. The substitution of the electron-releasing halide, Cl^-, with the electron-withdrawing ligand, py, dramatically influences the electronic absorption spectra of the complexes. An average blue shift of 50 nm is observed in the Ru $\rightarrow$ BL CT transitions between the Cl^- and py series. In going from $[(tpy)RuCl(dpp)]^+$ to $[(tpy)Ru(py)(dpp)]^{2+}$, the $Ru^{II/III}$ couple (HOMO) shifts to more positive potentials. The substitution does not significantly affect the LUMO, as the $dpp^{0/-}$ couple remains nearly constant. The blue shift in the MLCT transition is a result of the stabilization of the metal (dπ) level upon substitution with an electron-withdrawing substituent and is observed in the complexes bridged by dpq and dpb.

A similar series of complexes, $[Ru(tpy)(bpy)X]^{n+}$, was synthesized with X = CH_3CN, NO, py, NO_2, 4-Ph-py[15], Cl, PPh_3, CO, phenothiazine, *N*-methylphenothiazine[16], CN, H_2O[17], NH_3 and SCN[18]. As in the previous

example, the identity of X in the sixth coordination site dramatically influences the energy of the MLCT transition due to variations in the energy of the Ru (dπ) HOMO. The shift is consistent with an observed change in the $Ru^{II/III}$ redox couple, dependent on X.

Polyazine BLs play an important role in the design multimetallic complexes. The BL and metals influence both the structure of the complex and the degree of electronic communication between metal atoms. The study of electron and energy transfer in these complexes is a fundamental concern for the development of useful systems exploiting these properties. Dinuclear complexes containing Pt^{II} linked to Ru^{II} chromophores are interesting for many reasons.[4,19] Both the reactivity of the unsaturated coordination sphere and the DNA binding activity of *cis*-$PtCl_2$ are sparsely studied areas in the field of inorganic photochemistry.[20]

Interactions of Cisplatin and DNA

DNA is a biomacromolecule made up of many deoxyribonucleotide monomers.[21] Each nucleotide comprises a nitrogenous base, a sugar, and one or more phosphate groups. The sugar-phosphate groups are linked end-to-end (5'-3') and make up the backbone of the double-helix. Two strands are held together with hydrogen bonds between complimentary nitrogenous bases; guanine/cytosine and adenine/thiamine (Figure 8). The strands are coiled about a common axis to form the double helix with the base pairs stacked one above the other in the interior. The diversity found in the quaternary structure of DNA, major and minor groove, hydrophobic, and hydrophilic region, and a polyanionic charge, leads to the possibility for several types of interactions with foreign species. These include ionic bonding in the major and minor groove, intercalation between the stacked bases, and covalent bonding.

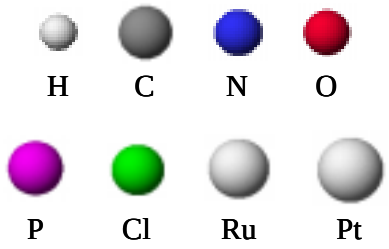

Figure 7. Atom color assignments used in CAChe molecular models.

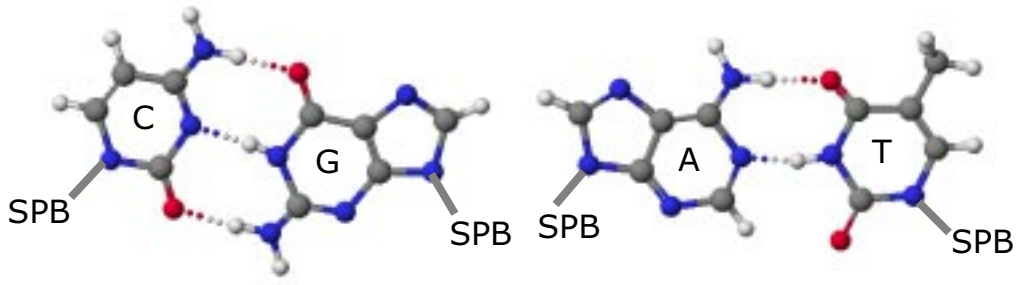

Figure 8. H-bonding interactions between guanine and cytosine, adenine and thiamine (SPB = sugar phosphate backbone).

Cisplatin coordinates to DNA primarily through N-7 of guanine to form a 1,2-intrastrand adduct (Figure 9).[22] The formation of these adducts disrupts base pairing, and the resulting destacking causes the DNA helix to become kinked. The 1,2-intrastrand adducts formed are important for the anticancer activity of cisplatin. It is believed the binding affects replication, transcription, and repair mechanisms.[20] Despite its success, cisplatin has several disadvantages that include severe toxicity and tumor resistance. Therefore, efforts continue toward the development of improved Pt antitumor drugs. One approach to the design of second-generation Pt drugs follows a set of structure-activity relationships summarized by Cleare and Hoeschele.[22] For Pt complexes to show anti-tumor activity, the Pt^{II} or Pt^{IV} complex should have a *cis* geometry of the general form *cis*-$[PtX_2(Am)_2]$ or

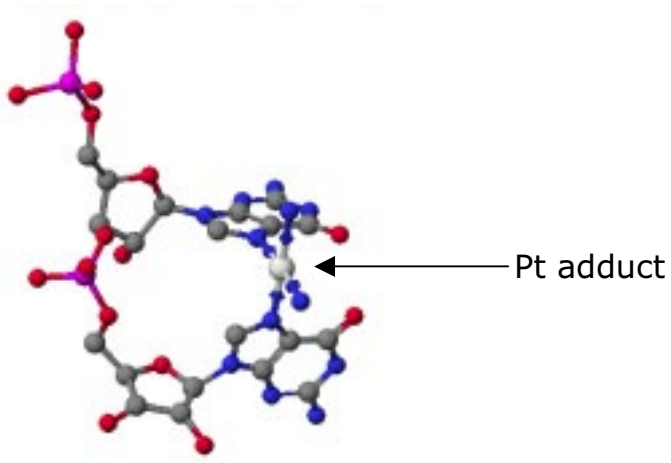

Figure 9. Intrastrand adduct formed between ciplatin and a guanasine dimer.

cis-$[PtX_2Y_2(Am)_2]$ where X is the leaving group and Am is an inert amine with at least one N-H moiety. Recently, other strategies have evolved[20] that include the use of sterically hindering ligands ,[23] the addition of biologically-active carrier ligands,[24] and abandoning the *cis*-chloride motif .[25]

Survey of Existing Ru^{II}-Pt^{II} Polypyridyl Complexes.

Examples of polyazine-bridged Ru-Pt complexes can be found in the literature. Most deal primarily with synthesis. The spectroscopic and electrochemical data is summarized in Table 3. All work on polypyridyl-bridged Ru-Pt complexes to date focuses on the $[Ru(bpy)_3]^{2+}$ moiety. Like the prototype, the electronic absorption spectra of these complexes are dominated by IL transitions in the UV region and Ru (d π) → L (π^*) CT transitions in the visible region. Various degrees of perturbation are observed in the spectra and electrochemistry with bimetallic formation and is dependent on the type of BL and metals attached. When Ru and Pt are bridged through a rigid, conjugated ring, the greatest perturbations are observed. Rillema first studied the Ru-Pt complex $[(bpy)_2Ru(bpm)PtCl_2]^{2+}$

Table 3. Electrochemistry and electronic absorption spectroscopy for polyazine bridged Ru-Pt complexes.

Complex	$E_{½}^{ox}$ (V)	$E_{½}^{red}$ (V)	λ_{max}^{abs} (nm)
$[(bpy)_2Ru(Mebpy^*\text{-}Mebpy)PtCl_2]^{2+}$ [a]	1.19	-1.27 ($Mebpy^{0/-}$) -1.38 ($bpy^{0/-}$)	457 Ru → bpy CT
$[(bpy)_2Ru(bpy^A\text{-}bpy^B)PtCl_2]^{2+}$ [b]	0.92	-1.44 -1.78 -1.95 -2.12	455 Ru → bpy^A CT
$[(bpy)_2Ru(bpy)_2(bpy^B\text{-}bpy^A)PtCl_2]^{2+}$ [b]	1.05	-1.38 -1.73 -1.95 -2.18	452 Ru → bpy^B CT
$[(bpy)_2Ru(bpm)PtCl_2]^{2+}$ [a]	1.35	-0.34 ($bpm^{0/-}$) -1.01 ($bpy^{0/-}$)	571 Ru → bpm CT
$[(bpy)_2Ru(dpp)PtCl_2]^{2+}$ [c]	1.57	-0.54 ($dpp^{0/-}$) -1.11 ($dpp^{-/2-}$) -1.49 ($bpy^{0/-}$)	509 Ru → dpp CT
$[(bpy)_2Ru(dpq)PtCl_2]^{2+}$ [d]	1.72	-0.28 ($dpq^{0/-}$) -0.82 ($dpq^{0/-}$)	582 Ru → dpq CT
$[(bpy)_2Ru(dpb)PtCl_2]^{2+}$ [d]	1.61	-0.11 ($dpb^{0/-}$) -0.75 ($dpb^{0/-}$)	630 Ru → dpb CT

[a] Data from ref. 26, 27 Potentials vs. SCE/propylene carbonate/TEAP.
[b] Data from ref. 28 Potentials vs. Ag/AgCl/ acetonitrile/TBAH.
[c] Data from ref. 29,30 Potentials vs. Ag/$AgNO_3$/acetonitrile/TBAH.
[d] Data from ref. 31,32 Potentials vs. Ag/AgCl/ acetonitrile/TBAH.

(bpm = 2,2′-bipyrimidine).[26] The monometallic precursor, $[Ru(bpy)_2(bpm)]^{2+}$, has a Ru(dπ) → bpm(π*) CT centered at 484 nm. The addition of electron deficient $PtCl_2$ red shifts the MLCT to 571 nm. The $Ru^{II/III}$ couple is relatively unaffected by Pt coordination with only a 10 mV change in the oxidation potential. The first reduction potential is significantly altered. $[Ru(bpy)_2(bpm)]^{2+}$ undergoes a $bpm^{0/-}$ based reversible one-electron reduction at −1.01 V (vs. SCE). Pt coordination shifts this potential more positive to −0.34 V. The electrochemical results indicate the change in the energy of the MLCT is due to a stabilization of the bpm π* acceptor orbitals.

Yam[29,30] reported the properties of the complex $[(bpy)_2Ru(dpp)PtCl_2]^{2+}$ while Brewer[19,31,32] expanded the series to include $[(bpy)_2Ru(dpq)PtCl_2]^{2+}$ and $[(bpy)_2Ru(dpb)PtCl_2]^{2+}$. The MLCT absorption bands for the bimetallic are red-shifted relative to the respective monometallic precursor. In this series, the $Ru^{II/III}$ redox couple is affected by $PtCl_2$ coordination. The $Ru^{II/III}$ redox couple for $[Ru(bpy)_2(BL)]^{2+}$ occurs at 1.54 V (vs. $Ag/AgNO_3$)[29], 1.47 V (vs. Ag/AgCl), and 1.48 V (vs. Ag/AgCl)[31] for dpp, dpq, and dpb, respectively. Bimetallic formation shifts the redox couple to more positive potentials. An irreversible Pt oxidation is reported in these complexes at the same potential as the $Ru^{II/III}$ couple. This might account for the seemingly disparate values reported by the two groups.

The effect of Pt coordination on the BL reduction processes is greater than that of the $Ru^{II/III}$ couple. For the monometallic species, the first reduction process is a $BL^{0/-}$ couple and occurs at −1.06 V (dpp), -0.72 V (dpq), and −0.62 V (dpb). The second reduction processes are $bpy^{0/-}$. Upon Pt coordination, the $BL^{0/-}$ reduction potentials are shifted cathodic by approximately 500 mV. In addition, the $BL^{-/2-}$ couple is shifted cathodic and occurs before the terminal $bpy^{0/-}$ couple.

The bimetallic species containing BLs that do not connect the metal atoms through conjugated, rigid ligands do not experience the same changes in their spectroscopic and electrochemical properties relative to their monometallic precursors. Rillema reported the spectroscopic and electrochemical data for $[(bpy)_2Ru(Mebpy\text{-}Mebpy)PtCl_2]^{2+}$.[27] The lowest energy absorption is a Ru ($d\pi$) $\rightarrow$ bpy (π^*) CT transition at 457 nm. Due to the electron-rich methyl group and saturated linker of the BL, the π^* orbitals are destabilized, increasing the energy of the Ru ($d\pi$) $\rightarrow$ BL (π^*) CT transition to 360 nm. The electronic absorption spectrum of $[Ru(bpy)_2(Mebpy\text{-}Mebpy)]^{2+}$ and the Ru-Pt product are identical with the exception of a Pt ($d\pi$) $\rightarrow$ Mebpy (π^*) CT transition at 324 nm observed in the bimetallic complex.[27]

Of these examples, only the $[(bpy)_2Ru(BL)PtCl_2]^{2+}$ (BL = dpq and dpb) series has been tested for DNA binding affinity.[19,32] Brewer reported results from agarose gel electrophoresis studies designed to assess DNA binding.[19,32] Various concentrations of bimetallic complex and DNA were incubated for 4 hrs. Adduct formation was assessed by comparing the DNA-bimetallic migration rate to that of free DNA and two known DNA binding agents, cisplatin[33] and $\{[PtCl(NH_3)_2]_2(\mu\text{-}NH_2(CH_2)_6NH_2)\}^{2+}$.[34] The complexes showed a general retardation of band migration due to adduct formation. The effect for $[(bpy)_2Ru(BL)PtCl_2]^{2+}$ was more pronounced than that for cisplatin and $\{[PtCl(NH_3)_2]_2(\mu\text{-}NH_2(CH_2)_6NH_2)\}^{2+}$. No change in migration rate was observed for the monometallic precursors, indicating adduct formation occurs through the *cis*-$PtCl_2$ moiety.

CHAPTER 2: EXPERIMENTAL

Materials

The ligands 2,3-*bis*(2′-pyridyl)pyrazine (dpp) and 2,2′:6′,2″-terpyridine (tpy) were purchased from Aldrich Chemical Company and used as received. Ruthenium trichloride hydrate ($RuCl_3 \cdot xH_2O$) and potassium tetrachloroplatinate were received from Johnson Matthey/Alfa-Aesar. Adsorption alumina (80-200) was purchased from Fisher Scientific. The supporting electrolyte for the electrochemical studies, tetrabutylammonium hexafluorophosphate (Bu_4NPF_6), was prepared by the metathesis of tetrabutylammonium bromide and potassium hexafluorophosphate. The electrolyte was recrystallized from hot ethanol (twice), dried in a vacuum oven, and stored in a nitrogen-filled glove box. HPLC-grade acetonitrile was purchased from Mallinckrodt and used for the electrochemical and spectroscopic studies. $Ru(tpy)Cl_3$[35] and $PtCl_2(dmso)_2$ (dmso = dimethylsulfoxide)[36] were prepared as previously reported.

Methods

Chromatography. The ruthenium precursors synthesized in this study were purified by alumina column chromatography. It was important that the alumina has not been activated or the complexes will bind irreversibly and not elute. Pyrex chromatography columns measuring 180 x 2.5 (O.D.) cm with a coarse glass frit bottom were filled to within 7 cm of the top with the eluting solvent and 1 cm of washed sea sand. Alumina was poured slowly and continuously into the column while the solvent elutes from the bottom. The rate was adjusted so that the loss of solvent volume was replaced with alumina to maintain a constant volume. This technique insures consistent packing of the alumina bed and an efficient separation. Sea sand (1 cm)

was added to the top of the alumina bed and the solvent allowed to elute until just covering the sand. Samples were prepared with the same solvent used to prepare the column and no more than 10-15 ml of the concentrated sample was introduced to a single column. The prepared sample was gently layered onto the top of the column with a pipette, allowed to enter the bed by opening the stopcock, and gently adding more solvent as the sample migrates down the column. Because these complexes were strongly colored, it was a simple matter to separate the eluting bands by visual inspection. The product bands were collected, concentrated by rotary evaporation, and precipitated by addition to diethyl ether. Successive separations on columns were sometimes necessary to fully separate the product from other components of the reaction.

NMR Spectroscopy. Proton NMR spectra were recorded on a JEOL Eclipse + 500 MHz spectrometer using the solvent (CD_2Cl_2) as an internal reference.

FAB-Mass Spectrometry. Mass spectral analysis was performed by a Fisons VG Quattro I, triple-stage quadrapole mass spectrometer equipped with a cesium ion gun. A *m*-nitrobenzyl alcohol/acetonitrile mixture served as the matrix.

Electrochemistry. A Bioanalytical Systems, Inc. 100W electrochemical workstation was used to generate cyclic voltammograms. In all cases, a 0.1 M Bu_4NPF_6 in acetonitrile serves as the supporting electrolyte. The three-electrode system consists of a 1.9 mm platinum disk working electrode, a platinum wire auxiliary electrode, and a Ag/AgCl reference electrode with a Vycor glass tip (0.286 V vs. NHE). The reference electrode was calibrated against the ferrocene/ferrocenium couple reported as 0.665 V vs. NHE in a 0.1 M Bu_4NPF_6/acetonitrile solution.[37] The platinum electrode was polished between each scan and the solutions deoxygenated by bubbling with argon for 20 min.

Electronic Absorption Spectroscopy. Spectra were generated at room temperature in a 1-cm quartz cuvette using a Hewlett Packard 8452 diode array spectrometer with 2-nm resolution and a spectral range of 190 to 820 nm. Data was acquired with Hewlett Packard UV-Vis Chemstation software (Rev. A. 02.05).

Preparation and Purification of Plasmid DNA. Plasmid DNA, pBluescript, was amplified and purified from *Escherichia coli* strain JM109 according to established methods.[38] Plasmids were isolated using an alkaline lysis procedure, purified in a cesium chloride gradient, and then extensively dialyzed against TE ([10 mM Tris (trishydroxymethyl)aminomethane], 1 mM EDTA, pH 7.5). Following concentration by ethanol precipitation, the DNA was stored in TE at 4 ^{o}C. Plasmid DNA was linearized by overnight incubation at 37 ^{o}C with *Eco*R1 endonuclease. Typically, 200 ug of plasmid DNA was combined with *Eco*RI (3 *µl*, 240 U) and 20 *µl* of 10X buffer in a total volume of 200 *µl*. Protein was removed by extracting with phenol/0.1% hydroxyquinoline (equilibriated with TE pH 8) and 24:1 chloroform /isoamyl alcohol. The DNA was then precipitated with NaCl and ethanol, resuspended in deionized water, and stored at 4 ^{o}C. The pBluescript plasmid was composed of 2958 base pairs and has a GC content of 50.2%.

Preparation of Molecular Weight Standards. Molecular weight standards for non-denaturing agarose gel electrophoresis were prepared by digestion of bacteriophage lambda DNA with *Hin*dIII endonuclease. Lambda DNA (50 ug, 100 µl of 500 ug/ml stock solution) was combined with Hind *III* (2 µl, 160 U) in 258 µl of H_2O buffered with 10X buffer (40 µl) and incubated for 12 hrs at 37 ^{o}C. Upon completion, 100 µl of 6X type III dye was added and the solution stored at 4 ^{o}C.[39]

Reactions of Metal Complexes with Plasmid DNA. The concentration of the linearized plasmid DNA solution was determined spectrophotometrically (1 AU = 50 µg DNA/ml at 258 nm).[40] Concentrations of metal solutions

were determined using the known extinction coefficients for [(tpy)RuCl(BL)$PtCl_2$](PF_6) ($\varepsilon = 14.9 \times 10^3\ M^{-1}cm^{-1}$ at 544 nm for dpp, 10.0 x $10^3\ M^{-1}cm^{-1}$ for dpq, and 9.89 x $10^3\ M^{-1}cm^{-1}$ for dpb). All reactions contain 1 µg of linearized plasmid DNA and 10 mM sodium phosphate, pH 7 in a total volume of 100 µl. The samples were analyzed by electrophoresis in 300 ml agarose gels (0.8% agarose, 89 mM Tris, 89 mM boric acid, pH 8) at 104 V for 1.5 hrs, with recirculation of the buffer.[32] Gels were then stained in 0.5 ug/ml ethidium bromide for 1 hr and photographed with UV illumination. Polaroid prints were scanned using digital flatbed scanner.

Synthesis

2,3-*bis*(2'-pyridyl)quinoxaline. 2,3-*Bis*(2'-pyridyl)quinoxaline (dpq) was synthesized by a modification of a previously-published method.[41] 2, 2'-pyridyl (4.24 g, 20.0 mmol) and 2,3-diaminephenylene (2.16 g, 20.0 mmol) were heated at reflux in 20 ml of ethanol for 2 hrs. The product forms white crystals as the solution cools to room temperature. The product was collected by vacuum filtration. Successive recrystallization from hot ethanol affords the pure product confirmed by ^{1}H NMR. Yield: 90% (5.12 g, 18.0 mmol)

2,3-*bis*(2'-pyridyl)benzoquinoxaline. Modification of the dpq synthesis affords 2,3-*bis*(2'-pyridyl)benzoquinoxaline (dpb).[42] 2,3-diaminonapthalene (3.16 g, 20.0 mmol) was substituted for 2,3-diaminophenylene. The crude product was purified by dissolving in a minimal amount of methylene chloride and eluting from a column packed with 5 cm of alumina (as described previously). The only band to elute was the yellow product. Purity was confirmed by ^{1}H NMR. Yield: 89% (5.95 g, 0.178 mmol).

[(tpy)RuCl(dpp)](PF_6). [(tpy)RuCl(dpp)](PF_6) was prepared by a modification of a previously-published method.[13] Ru(tpy)Cl_3 (0.824 g, 1.87 mmol), dpp (0.599 g, 2.56 mmol) and LiCl (0.100 g, 2.38 mmol) were

heated under an argon atmosphere for 5 h at reflux in 100 ml of a 2:1 ethanol/deionized water mixture. Addition of 8 ml triethylamine facilitates the reduction of Ru^{III}. The reaction mixture changes from brown to maroon and was precipitated by addition to 40 ml of a saturated solution of KPF_6. The dark precipitate was collected by vacuum filtration using a 30 ml fine-porosity fritted funnel. The product was purified by alumina chromatography prepared with 3:2 (vol./vol.) toluene/acetonitrile (as previously described). The first band to elute (red) was the desired product and was collected. The second band to elute was orange and determined to be $[(tpy)Ru(CH_3CN)(dpp)](PF_6)_2$. Several blue bands remained on the column and are assumed to be polymetallic complexes, but are not yet characterized. Yield: 90% (1.26 g, 1.68 mmol).

$[(tpy)RuCl(dpq)](PF_6)$. $[(tpy)RuCl(dpq)](PF_6)$ was prepared by a modification of the synthesis of $[(tpy)RuCl(dpp)](PF_6)$, substituting dpq (0.727 g, 2.56 mmol) for dpp.[13] The purification was as above with the first band (purple) being collected. Yield: 90% (1.35 g, 1.68 mmol).

$[(tpy)RuCl(dpb)](PF_6)$. $[(tpy)RuCl(dpb)](PF_6)$ was prepared by a modification of the synthesis of $[(tpy)RuCl(dpp)](PF_6)$, substituting dpb (0.855 g, 2.56 mmol) for dpp.[13] The purification was as above using a 2:1 (vol./vol.) toluene/acetonitrile eluant. The first band (blue) was collected. Yield: 88% (1.40 g, 1.64 mmol).

General Note on Ru-Pt Bimetallic Complexes. The successful synthesis and purification of the bimetallic complexes depends on the purity of the starting materials and the correct stoichiometry of the reaction mixture. This was due, in part, to the labile nature of the Pt-Cl bonds, which renders absorption chromatography unusable. Therefore, purification relies on the differential solubility of the precursors and products. In addition, increased reaction time leads to Pt^0 deposition on the reaction vessel.

[(tpy)RuCl(dpp)PtCl$_2$](PF$_6$). [(tpy)RuCl(dpp)PtCl$_2$](PF$_6$) was prepared by heating at reflux in 10 ml of ethanol [(tpy)RuCl(dpp)](PF$_6$) (0.150 g, 0.200 mmol) and PtCl$_2$(dmso)$_2$ (0.089 g, 0.21mmol). During the 1 hr reaction time, the solution changed from red to purple. Once the reaction mixture has cooled to room temperature, the purple product precipitated and was separated by vacuum filtration on a fine-porosity fritted funnel. The product was washed with two 10 ml portions of ethanol and 10 ml chloroform. Washing the frit with 30 ml acetonitrile allows the product to be collected as the filtrate. The volume of the purple filtrate was reduced to 15 ml by rotoevaporation and precipitated by addition to 60 ml diethyl ether. Yield 90% (182 mg, 0.180 mmol). FAB-MS (nitrobenzyl alcohol matrix), *m/z*: 870, [(tpy)RuCl(dpp)PtCl$_2$]$^+$; 834, [(tpy)RuCl(dpp)PtCl]$^+$; 799, [(tpy)RuCl(dpp)Pt]$^+$; 763, [(tpy)Ru(dpp)Pt]$^+$; 604, [(tpy)RuCl(dpp)]$^+$; 568, [(tpy)Ru(dpp)]$^+$.

[(tpy)RuCl(dpq)PtCl$_2$](PF$_6$). [(tpy)RuCl(dpq)PtCl$_2$](PF$_6$) was prepared by a modification of the reaction for [(tpy)RuCl(dpp)PtCl$_2$](PF$_6$), using [(tpy)RuCl(dpq)](PF$_6$) (0.160 g, 0.200 mmol). The resulting blue product was obtained in an 85% yield (182 mg, 0.170 mmol). FAB-MS (nitrobenzyl alcohol matrix), *m/z*: 920, [(tpy)RuCl(dpq)PtCl$_2$]$^+$; 884, [(tpy)RuCl(dpq)PtCl]$^+$; 848, [(tpy)RuCl(dpq)Pt]$^+$; 811, [(tpy)Ru(dpq)Pt]$^+$; 654, [(tpy)RuCl(dpq)]$^+$; 618, [(tpy)Ru(dpq)]$^+$.

[(tpy)RuCl(dpb)PtCl$_2$](PF$_6$). [(tpy)RuCl(dpb)PtCl$_2$](PF$_6$) was prepared by a modification of the reaction for [(tpy)RuCl(dpp)PtCl$_2$](PF$_6$), using [(tpy)RuCl(dpb)](PF$_6$) (0.170 g, 0.200 mmol). The resulting green product was obtained in an 80% yield (178 mg, 0.160 mmol). FAB-MS (nitrobenzyl alcohol matrix), *m/z*: 970, [(tpy)RuCl(dpb) PtCl$_2$]$^+$; 934, [(tpy)RuCl(dpb)PtCl]$^+$; 899, [(tpy)RuCl(dpb)Pt]$^+$; 862, [(tpy)Ru(dpb)Pt]$^+$; 704,[(tpy)RuCl(dpb)]$^+$; 668, [(tpy)Ru(dpb)]$^+$.

CHAPTER 3: RESULTS & DISCUSSION

Synthesis

The general method for the synthesis of $[(tpy)RuCl(BL)PtCl_2]^+$ is illustrated in Scheme 1. The synthesis takes advantage of a building block approach where each complex is built up by successively adding ligands and metals to the ruthenium supramolecular architecture. The ligands act as discrete scaffolds that contribute particular spectroscopic and electrochemical characteristics to the final complex. The interaction of the ligands and the metal atoms is weak enough that many of the prope rties of the ligands are maintained, but strong enough to give rise to new properties.[6] With this, the spectroscopic, electrochemical and structural attributes of the target complex are engineered through selection of modules particular to that task.

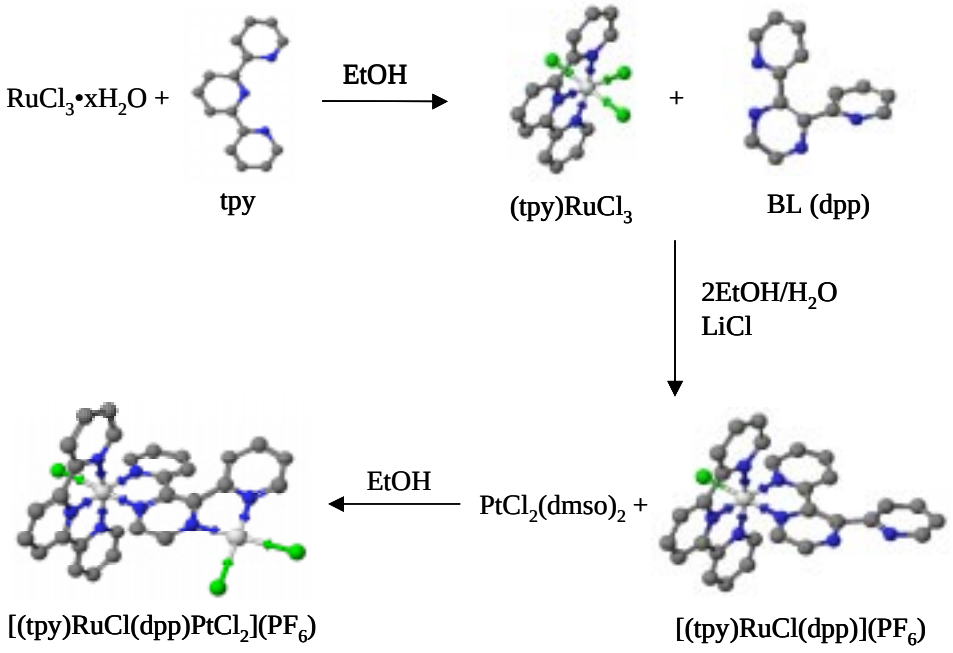

Scheme 1. Building block synthesis of $[(tpy)RuCl(BL)PtCl_2]^+$.

$Ru(tpy)Cl_3$ was synthesized as described by Meyer by heating at reflux in ethanol, $RuCl_3xH_2O$ and tpy.[35] The monometallic precursors, $[(tpy)RuCl(BL)](PF_6)$, were prepared by the modification of a previously-published method.[13] The addition of LiCl to the reaction mixture raised yields by 11% for dpp, 25% for dpq, and 25% for dpb by minimizing the formation of $[(tpy)Ru(CH_3CN)(BL)](PF_6)_2$. A persistent orange band observed during the chromatographic purification of the reaction mixture was suspected to be $[(tpy)Ru(CH_3CN)(dpp)](PF_6)_2$. Heating the orange byproduct in ethanol at reflux with LiCl for 30 min, gave a red precipitate that exhibits the same electrochemical, spectroscopic, and FAB-MS characteristics as $[(tpy)RuCl(dpp)](PF_6)$. The addition of excess Cl^- retarded the formation of the $[(tpy)Ru(CH_3CN)(BL)](PF_6)_2$.

The title complexes were synthesized by heating at reflux in ethanol, a 1:1.2 mole ratio of $[(tpy)RuCl(BL)](PF_6)$ and $PtCl_2(dmso)_2$. By monitoring the reaction spectroscopically, the reaction was found to be complete in 1 hr. This was observed as decay of the absorption band centered at 510 nm for dpp, 570 mn for dpq, and 595 nm for dpb and the appearance of an absorption band at 544 nm for dpp, 632 mn for dpq, and 682 nm for dpb. Measuring the reaction spectroscopically helped ensure complete product formation without the loss of the labile Ru-bound chloride or the reduction of Pt^{II}. The bimetallic complex was far less soluble than the ruthenium precursor and fell out of solution upon cooling the reaction mixture to room temperature. This was important as the $PtCl_2$ moiety irreversibly binds to alumina. Because alumina chromatography purification is not feasible, particular attention was paid to the stoichiometry and reaction conditions simplify purification process. After cooling to RT, the reaction solvent was slightly colored with the unreacted monometallic precursor, which was removed by filtration. The solid was washed with additional ethanol until the filtrate was clear. By washing the product through the frit with

acetonitrile, any Pt side products were removed. Flash precipitation of the acetonitrile solution in diethyl ether afforded an additional purification step. The product was dried and collected for characterization by FAB-MS, electrochemistry, and electronic absorption spectroscopy.

The tpy ligand is typically used to simplify the stereochemistry of Ru-polypyridyl complexes. Using only tridentate ligands leads to symmetric rod-like complexes that eliminate the Δ and Λ isomers of *bis*-chelated complexes and aid the NMR characterization of the complexes. The combination of tpy and the *bis*-bidentate BL series does not simplify the stereochemistry of $[(tpy)RuCl(BL)PtCl_2]^+$ but is used to provide an additional route for tuning the spectroscopic and electrochemical properties of the complex. The sixth coordination site of Ru has an easily-substituted Cl^- that adds another degree of synthetic variability. The two configurational isomers, chloride *cis* or *trans* to the pyrazine ring (Figure 10), are presumably both synthesized. Neither isomer is lost in the current synthetic method and will carry through to the bimetallic products. The isomers of $[(tpy)RuCl(BL)]^+$ were indistinguishable by FAB-MS, electrochemistry or electronic absorption spectroscopy.[13]

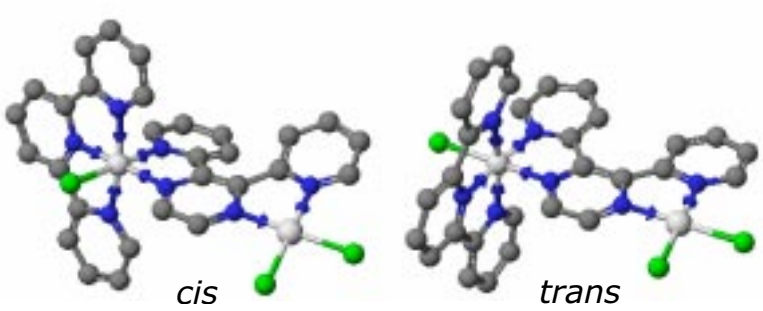

Figure 10. *cis*- and *trans*- Isomers of $[(tpy)RuCl(dpp)PtCl_2]^+$.

In this study, a series of BLs was investigated (Figure 1). The build up of conjugated rings about the central pyrazine ring alters the electronic properties of the ligand while maintaining the diimine bridging coordination

mode.[14] Because these changes are introduced in a regular manner, the characterization of these complexes is simplified. Direct comparisons of the spectroscopy and electrochemistry of each complex can be followed as a function of ligand choice. This helps in the assignment of transitions that occur in the electronic absorption spectra and redox couples in the electrochemistry.

FAB Mass Spectra

The FAB-MS data for $[(tpy)RuCl(BL)PtCl_2](PF_6)$ is summarized in Table 4. All spectra exhibit the molecular ion peak, $[M - (PF_6)]^+$, and expected fragmentation peaks corresponding to the loss of chloride, platinum, and intact ligands (i.e. tpy & BL). A particular ion displays a group of closely-spaced peaks in the mass spectrum due to the natural occurrence of isotopes. The FAB mass spectra are included in Appendix 1, 2,and 3 for the bimetallic complexes (pages 44-49).

The $[(tpy)RuCl(dpp)PtCl_2](PF_6)$ mass spectrum shows five groups of peaks at high mass to charge ratio. The peak at 870 corresponds to the molecular ion, $[(tpy)RuCl(BL)PtCl_2]^+$. The lower mass peaks at 835, 799, and 764 are separated by the mass of chloride and are assigned $[(tpy)RuCl(BL)PtCl]^+$, $[(tpy)RuCl(BL)Pt]^+$, and $[(tpy)Ru(BL)Pt]^+$, respectively. The peak at 604 differs from the molecular ion by 266. This is due to the loss of platinum and two chlorides and is therefore assigned $[(tpy)RuCl(BL)]^+$. Loss of chloride from $[(tpy)RuCl(BL)]^+$ gives the final high mass peak at 569. Taken together, the molecular ion peak and readily-explained fragment peaks lend strong support for the synthesis of $[(tpy)RuCl(dpp)PtCl_2](PF_6)$.

Table 4. FAB Mass spectral data for $[(tpy)RuCl(BL)PtCl_2](PF_6)$ where BL = dpp, dpq, and dpb.[a]

	dpp		dpq		dpb	
	m/z	%	*m/z*	%	*m/z*	%
$[(tpy)RuCl(BL)PtCl_2]^+$	870	28	920	75	970	45
$[(tpy)RuCl(BL)PtCl]^+$	835	90	885	90	935	60
$[(tpy)RuCl(BL)Pt]^+$	799	40	849	75	899	47
$[(tpy)Ru(BL)Pt]^+$	764	35	814	40	864	20
$[(tpy)RuCl(BL)]^+$	604	100	654	100	704	100
$[(tpy)Ru(BL)]^+$	569	90	619	75	669	50

[a] tpy = 2,2′:6′,2″-terpyridine, dpp = 2,3-*bis*(2′-pyridyl)pyrazine, dpq = 2,3-*bis*(2′-pyridyl)quinoxaline, and dpb = 2,3-*bis*(2′-pyridyl)benzoquinoxaline

The mass spectrum of $[(tpy)RuCl(dpq)PtCl_2](PF_6)$, which differs from $[(tpy)RuCl(dpp)PtCl_2](PF_6)$ by 4 carbon and 2 hydrogen atoms, exhibits five groups of peaks. The mass peak at 920 corresponds to the molecular ion $[(tpy)RuCl(dpq)PtCl_2]^+$. Loss of chloride gives the next three lower mass peaks at 885, 849, and 814 corresponding to $[(tpy)RuCl(dpq)PtCl]^+$, $[(tpy)RuCl(dpq)Pt]^+$, and $[(tpy)Ru(dpq)Pt]^+$ respectively. The peak at 654 is due to loss of $PtCl_2$ from the molecular ion and is described as $[(tpy)RuCl(dpq)]^+$. Loss of chloride from $[(tpy)RuCl(dpq)]^+$ gives the mass peak at 619. The combination of the molecular ion peak and readily-explained fragment peaks lends strong support for the synthesis of $[(tpy)RuCl(dpq)PtCl_2](PF_6)$.

The addition of 8 carbon and 4 hydrogen atoms to the bridging ligand, dpp, accounts for the 50 AMU difference in $[(tpy)RuCl(dpp)PtCl_2](PF_6)$ and $[(tpy)RuCl(dpb)PtCl_2](PF_6)$. The mass spectrum of $[(tpy)RuCl(dpb)PtCl_2](PF_6)$ shows five groups of peaks. The molecular ion peak, $[(tpy)RuCl(dpb)PtCl_2](PF_6)$, occurs at 970. Loss of chloride from the parent species accounts for the next three lower mass ions,

$[(tpy)RuCl(dpb)PtCl]^+$ at 935, $[(tpy)RuCl(dpb)Pt]^+$ at 899, $[(tpy)Ru(dpb)Pt]^+$ at 864. The peak at 704 is due to loss of $PtCl_2$ from the molecular ion and is identified as $[(tpy)RuCl(dpb)]^+$. Loss of chloride from $[(tpy)RuCl(dpb)]^+$ gives the mass peak at 669. The combination of the molecular ion peak and readily-explained fragment peaks lends strong support for the synthesis of $[(tpy)RuCl(dpb)PtCl_2]^+$.

Electrochemistry

The cyclic voltammograms of $[(tpy)RuCl(BL)PtCl_2](PF_6)$ appear as Figure 11, Figure 12, and Figure 13 for BL = dpp, dpq, and dpb, respectively. The electrochemical behavior of these complexes is characterized by a metal-based reversible oxidation and several ligand-based reductions (Scheme 2). The potential at which the bound ligands

$$[(tpy)Ru^{III}Cl(BL)PtCl_2]^{2+}$$
$$-1e^- \uparrow\downarrow +1e^-$$
$$^{\ddagger}[(tpy)Ru^{II}Cl(BL)PtCl_2]^{+}$$
$$-1e^- \uparrow\downarrow +1e^-$$
$$[(tpy)Ru^{II}Cl(BL^-)PtCl_2]$$
$$-1e^- \uparrow\downarrow +1e^-$$
$$[(tpy)Ru^{II}Cl(BL^{2-})PtCl_2]^-$$
$$-1e^- \uparrow\downarrow +1e^-$$
$$[(tpy^-)Ru^{II}Cl(BL^{2-})PtCl_2]^{2-}$$

Scheme 2. Electrochemical mechanism for $[(tpy)RuCl(BL)PtCl_2]^+$ (‡ = synthesized oxidation state).

undergo a reduction is expected to follow that of the free ligands, that is dpb > dpq > dpp > tpy. For the three bimetallic complexes, the first and second reduction processes are BL-based and occur at lower potentials than the

terminal tpy ligand reduction. The assignments are supported by the varying potentials observed for the first and second reduction and the constant reduction potential of the third in the series of complexes $[(tpy)RuCl(BL)PtCl_2]^+$ as the BL is varied (Table 5). Square wave voltammetry was used to assign the $tpy^{0/-}$ reduction potential as the quasi-reversible process is complicated by adsorption processes. The squarewave voltammograms are included in Appendix 4, 5, and 6 (pages 50 - 52).

The $[(tpy)RuCl(dpp)PtCl_2](PF_6)$ cyclic voltammogram, Figure 11, shows several electrochemical processes. The reversible oxidation at +1.14 V is assigned as a $Ru^{II/III}$ couple. The first and second reductions at −0.50 and −1.05 V are assigned as $dpp^{0/-}$ and $dpp^{-/2-}$ couples, respectively. The third reduction, seen in the squarewave volammogram at −1.43 V, is assigned $tpy^{o/-}$ (Appendix 4).

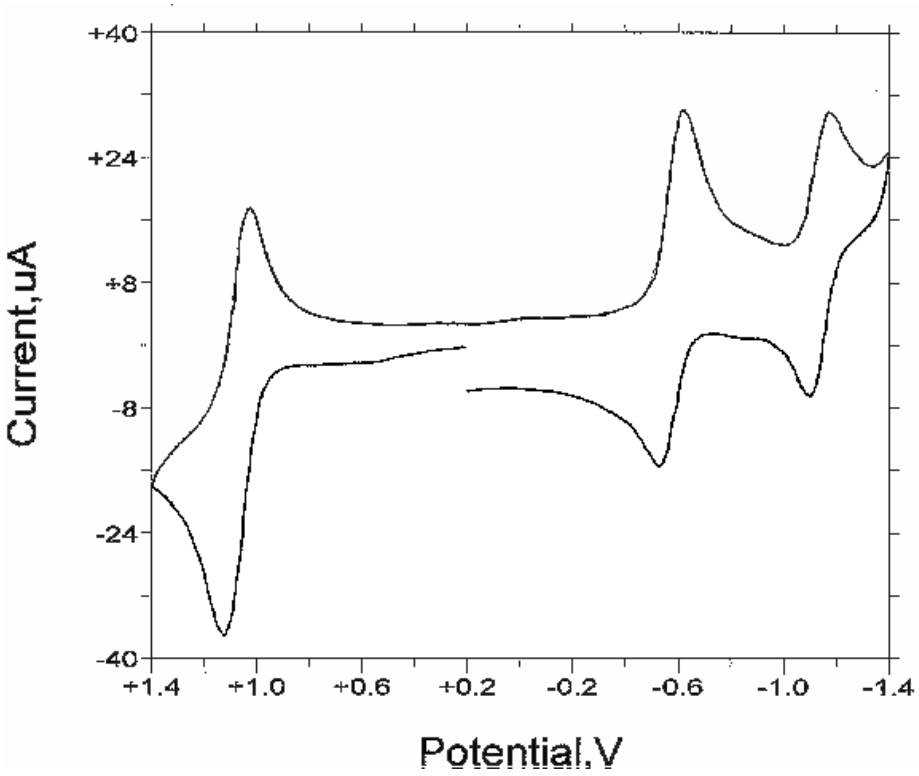

Figure 11. Cyclic voltammogram of $[(tpy)RuCl(dpp)PtCl_2](PF_6)$
Potentials reported in CH_3CN vs. Ag/AgCl (0.286 V vs. NHE).

The cyclic voltammogram of [(tpy)RuCl(dpq)PtCl$_2$](PF$_6$), Figure 12, is similar to that of the dpp bridged complex with significant shifts of the first and second reductive couple. These couples are BL-based and are seen at –0.32 V for dpq$^{0/-}$ and –0.84 V for dpq$^{-/2-}$. The third reduction at –1.49 V is assigned as tpy$^{o/-}$ (Appendix 5). The Ru$^{II/III}$ couple occurs at +1.10 V.

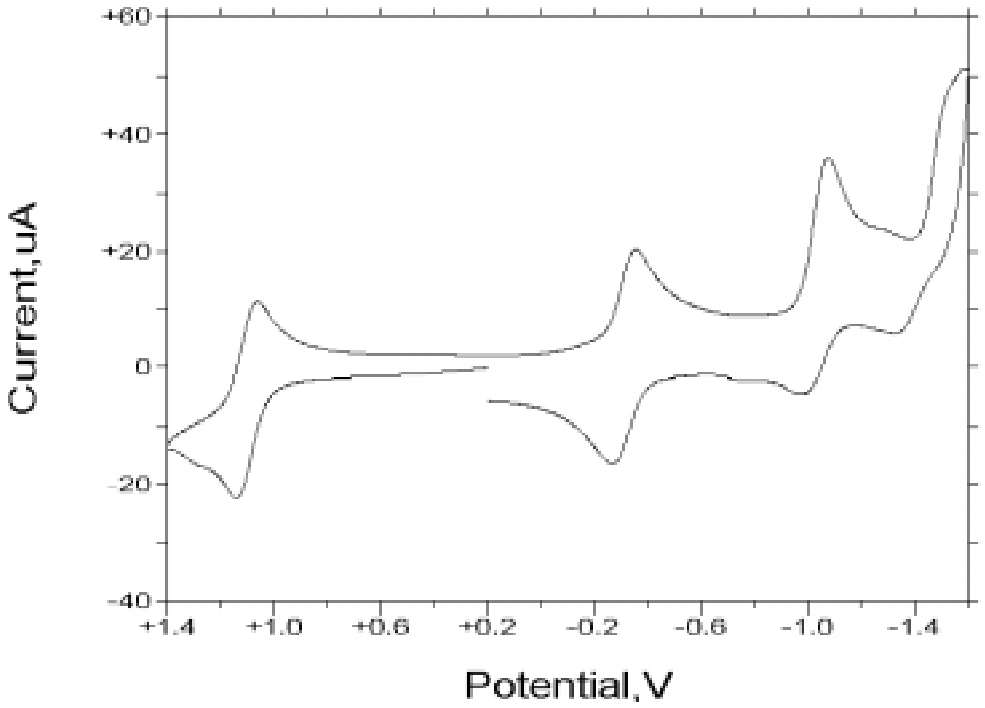

Figure 12. Cyclic voltammogram of [(tpy)RuCl(dpq)PtCl$_2$](PF$_6$) Potentials reported in CH$_3$CN vs. Ag/AgCl (0.286 V vs. NHE).

The cyclic voltammogram of [(tpy)RuCl(dpb)PtCl$_2$](PF$_6$), Figure 13, also exhibits dramatically shifted reduction couples compared to both the dpp and dpq analogues. These reductions occur at –0.20 and –0.75 V are assigned as dpb$^{0/-}$ and dpb$^{-/2-}$ based processes. The third reduction at –1.48 V is assigned as tpy$^{o/-}$ (Appendix 6). A Ru$^{II/III}$ oxidative couple is observed at +1.12 V.

The tpy-based reduction and Ru-based oxidation potentials remain nearly constant as the BL is varied through the [(tpy)RuCl(BL)PtCl$_2$]$^+$ series.

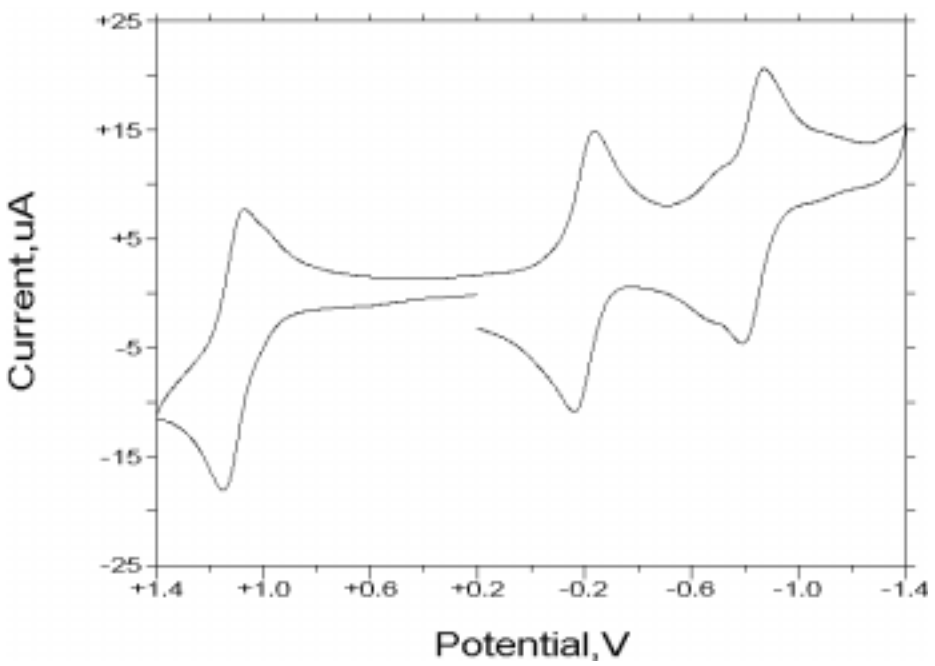

Figure 13. Cyclic voltammogram of $[(tpy)RuCl(dpb)PtCl_2](PF_6)$ Potentials reported in CH_3CN vs. Ag/AgCl (0.286 V vs. NHE).

The constant tpy reduction potentials (-1.47 V) indicate that changes in the complexes due to the BL, have a minor impact on the tpy ligand. The trend supports the assignment of the third reduction as tpy $^{0/-}$ based, and is observed in the complexes $[(tpy)RuCl(BL)](PF_6)$ and $[(tpy)Ru(py)(BL)](PF_6)_2$ (where py = pyridine).[13] The reduction potentials for tpy in these complexes vary little, ranging from -1.25 to – 1.27 V for the chloride series and –1.34 to –1.35 V for the py series. At first glance it seems peculiar that the tpy reduction for $[(tpy)RuCl(BL)](PF_6)$ occurs at a more positive potential than the title bimetallic complexes. The coordination of $PtCl_2$ is expected to remove electron density from Ru by the BL, thereby reducing electron density on tpy. The expected effect is a tpy reduction that occurs at a lower potential for the Ru-Pt bimetallics than for the monometallic precursors. The opposite is observed. The values reported for $[(tpy)RuCl(BL)](PF_6)$ correspond to the second reduction process for that complex, i.e. the $[(tpy)RuCl(BL^-)] + 1e^- \rightarrow [(tpy^-)RuCl(BL^-)]^-$ process. The values reported for

the title complexes correspond to the third reduction process, i.e. the $[(tpy)RuCl(BL^{-2})PtCl_2]^- + 1e^- \rightarrow [(tpy^-)RuCl(BL^{-2})PtCl_2]^{-2}$ process. The difference in redox order renders a direct comparison between the two series impossible.

Table 5. Cyclic voltammetric data for $[(tpy)RuCl(BL)PtCl_2](PF_6)$ were BL = dpp, dpq, and dpb.[a]

Complex	$E_{1/2}$ (V)[b]	Assignment
$[(tpy)RuCl(dpp)PtCl_2]^+$	+1.14	$Ru^{II/III}$
	-0.50	$dpp^{0/-}$
	-1.05	$dpp^{-/2-}$
	-1.43	$tpy^{0/-}$
$[(tpy)RuCl(dpq)PtCl_2]^+$	+1.10	$Ru^{II/III}$
	-0.32	$dpq^{0/-}$
	-0.91	$dpq^{-/2-}$
	-1.50	$tpy^{0/-}$
$[(tpy)RuCl(dpb)PtCl_2]^+$	+1.12	$Ru^{II/III}$
	-0.20	$dpb^{0/-}$
	-0.81	$dpb^{-/2-}$
	-1.51	$tpy^{0/-}$

[a] dpp = (2,3-*bis*(2-pyridyl)pyrazine, dpq = (2,3-*bis*(2-pyridyl)quinoxaline, dpb = (2,3-*bis*(2-pyridyl) benzoquinoxaline, and tpy = 2,2′:6′,2″-terpyridine.
[b] Potentials reported in CH_3CN solution with 0.1 M Bu_4NPF_6 and reported vs. Ag/AgCl (0.286 V vs. NHE).

The similarities of the Ru oxidation potentials (1.14 to 1.10 V vs. Ag/AgCl in CH_3CN) indicate nearly constant Ru-based dπ orbital energy levels. These oxidations are within the range of potentials observed in similar complexes. The $Ru^{II/III}$ couple for complexes containing only polypyridine ligands occurs around +1.5 V (vs. NHE).[6] Substituting one chloride in this type of complex to form $[Ru(tpy)(bpy)Cl]^+$ lowers the redox

couple to 1.05 V (vs. NHE).[16] The monometallic complexes, [(tpy)RuCl(BL)](PF_6), also exhibit a constant oxidation potential with an average $Ru^{II/III}$ couple of 1.04 V (vs. NHE) that varies by 40 mV through the BL series.[13]

Comparing the average ruthenium oxidation potentials of [(tpy)RuCl(BL)](PF_6) and the title Ru-Pt bimetallic complexes show a difference of 80 mV. The oxidation potentials for the bimetallic complexes are at more positive potentials due to the electron-withdrawing effect that platinum coordination imparts on the complex. Similar observations have been made in other Ru-Pt complexes and are summarized in Table 3.[26-29,31]

The largest electrochemical differences observed in [(tpy)RuCl(BL)$PtCl_2$]$^+$ lie in the redox potentials of the BL. These reductions are observed at −0.50 V dpp, −0.32 V dpq, and −0.20 V dpb for the first $BL^{0/-}$ reductive process and at −1.05 V dpp, −0.84 V dpq, and −0.75 V dpb for the second $BL^{-/2-}$ couple. The ease with which the bridging ligands in the bimetallic complexes are reduced follows the trend observed for the free ligands and aids in the assignment of the reduction process.[14] The monometallic precursors, [(tpy)RuCl(BL)]$^+$, also exhibit this trend with the first reduction potentials reported as -1.07 V dpp, -0.77 V dpq, and −0.61 V dpb. The differences in the first reduction potentials for [(tpy)RuCl(BL)](PF_6) and [(tpy)RuCl(BL)$PtCl_2$](PF_6) are large. Coordination of platinum stabilizes the BLs as observed by the shift in the reduction processes to more positive potentials. The stabilizing effect is also seen in the second reduction processes of the Ru-Pt complexes. For the three bimetallic complexes, the second reduction is also BL-based, occurring before the initial reduction of the terminal tpy ligand. The BLs of the monometallic precursors undergo only one reduction before the reduction of tpy. The presence of a second BL reduction prior to terminal ligand reduction in [(tpy)RuCl(BL)$PtCl_2$](PF_6) is

indicative of the bridging coordinative mode of the BLs and supports the bimetallic formulation of these compounds.[31]

In the complexes, $[(bpy)_2Ru(BL)PtCl_2]^{2+}$, the $Ru^{II/III}$ oxidation potential is complicated by the presence of an irreversible oxidation potential at similar potentials.[31] It is assumed the irreversible oxidation is Pt based. The presence of a Ru bound chloride in the title complexes shifts the $Ru^{II/III}$ redox couple anodic, away from the $Pt^{II/IV}$ oxidation potential (1.6 V vs. Ag/AgCl). In fact, a Pt oxidation is not seen in $[(tpy)RuCl(BL)PtCl_2]^+$ in the solvent window (2.0 to –2.0 V).

By altering the BL in the complex, $[(tpy)RuCl(BL)PtCl_2](PF_6)$, in a systematic way, periodic modifications of the redox processes are introduced and allows the assignment of all redox processes in the CH_3CN window. In addition, comparisons between the Ru-Pt bimetallics and monometallic precursors indicate that the only oxidation is $Ru^{II/III}$ based and that the presence of chloride shifts the $Ru^{II/III}$ couple more anodic. Through simple changes in the BLs, the energy of the LUMO is dramatically changed while the energy of the HOMO is relatively unaffected. The changes afford a method for tuning the spectroscopic properties of this type of complex as the MLCT transition is between these two MOs.

Electronic Absorption Spectroscopy

The electronic absorption spectra of ruthenium d^6 complexes with polypyridyl ligands displays intraligand $\pi \rightarrow \pi^*$ and $n \rightarrow \pi^*$ transitions as well as metal ($d\pi$) → ligand (π^*) charge transfer transitions. The $[(tpy)RuCl(BL)PtCl_2]^+$ title complexes are expected to exhibit these transitions-based on each polypyridyl ligand. Complete assignment of all bands in spectra is made difficult by the large number of transitions within a similar energy range. The complications include multiple $\pi \rightarrow \pi^*$ intraligand transitions and multiple Ru → tpy and Ru → BL charge transfer transitions.

Figure 14 is an overlay of the electronic absorption spectra of the three dpp, dpq, and dpb bridged Ru-Pt bimetallic complexes. A summary of the spectroscopic data can be found in Table 6.

The title complexes are good light absorbers and display many intense absorption bands. Intraligand transitions dominate the high-energy ultraviolet region of the spectrum. Two sets of peaks occur at the same wavelength for the bimetallic series. These are at 272 nm and 316 nm and assigned as tpy $\pi \rightarrow \pi^*$ transitions. The same peaks are seen in the spectra of the monometallic syntons, $[(tpy)RuCl(BL)]^+$, and occur at the same wavelength.[13] The peaks are red shifted from the 236 nm $\pi \rightarrow \pi^*$ transition of the free tpy ligand.[14]

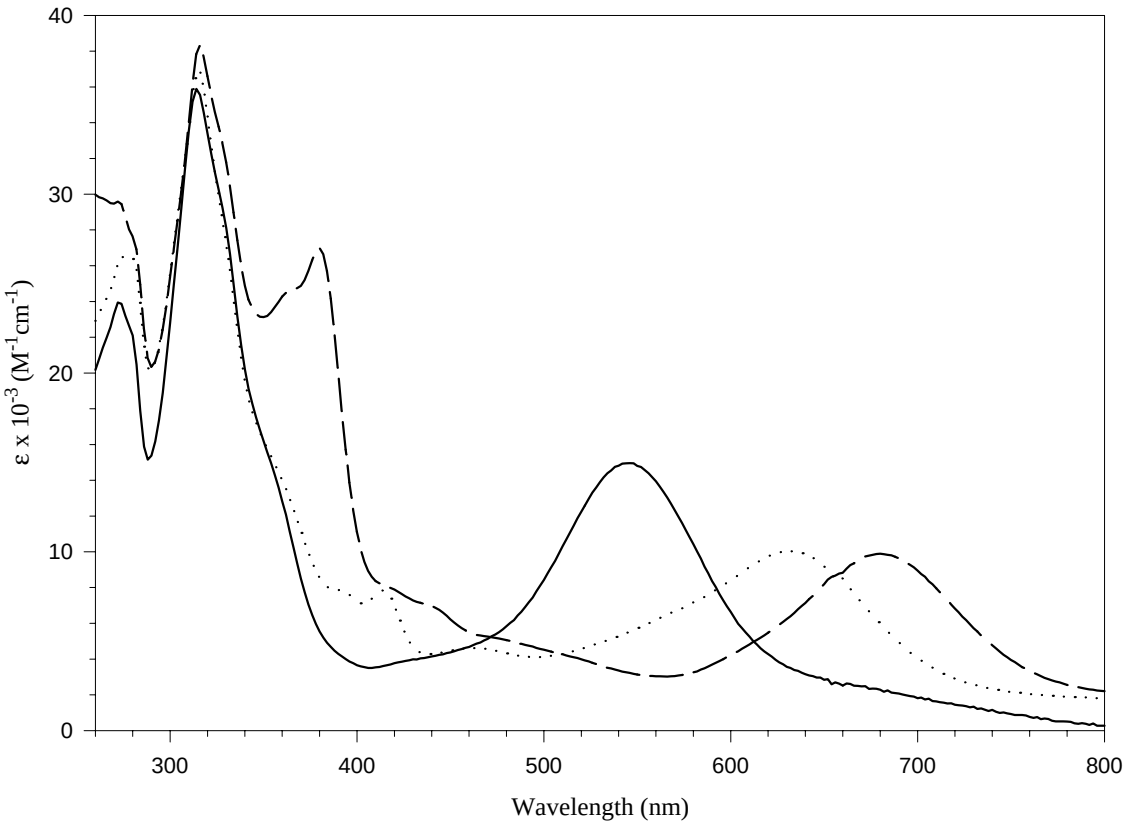

Figure 14. Electronic absorption spectra of $[(tpy)RuCl(BL)PtCl_2]^+$ in acetonitrile: BL = — dpp, ····· dpq, and – – dpb.

Bridging ligand $\pi \rightarrow \pi^*$ transitions are seen at 354 nm dpp, 362 nm dpq, and 380 nm dpb for the bimetallic complexes. These transitions occur at lower energy than the free ligand $\pi \rightarrow \pi^*$ transitions at 248 dpp, 268 dpq, and 290 nm dpb and the monometallic precursors in acetonitrile.[13,14] The red shifts in these $\pi \rightarrow \pi^*$ transitions displayed in the electronic absorption spectra of $[(tpy)RuCl(BL)PtCl_2]^+$ indicate stabilization of the BL π^* orbitals upon platinum coordination.

Table 6. Electronic absorption data for $[(tpy)RuCl(BL)PtCl_2]^+$ were BL = dpp, dpq, and dpb.[a]

Complex	λ_{max} (nm)	$\varepsilon \times 10^{-3}$ ($M^{-1}cm^{-1}$)	Assignment
$[(tpy)RuCl(dpp)PtCl_2]^+$	272	23.9	tpy $\pi \rightarrow \pi^*$
	316	35.6	tpy $\pi \rightarrow \pi^*$
	354	15.0	dpp $\pi \rightarrow \pi^*$
	544	14.6	Ru $\rightarrow$ dpp CT
$[(tpy)RuCl(dpq)PtCl_2]^+$	272	26.1	tpy $\pi \rightarrow \pi^*$
	316	36.9	tpy $\pi \rightarrow \pi^*$
	362	13.6	dpq $\pi \rightarrow \pi^*$
	632	10.0	Ru $\rightarrow$ dpq CT
$[(tpy)RuCl(dpb)PtCl_2]^+$	272	29.6	tpy $\pi \rightarrow \pi^*$
	316	38.3	tpy $\pi \rightarrow \pi^*$
	380	27.0	dpb $\pi \rightarrow \pi^*$
	682	9.86	Ru $\rightarrow$ dpb CT

[a] dpp = (2,3-*bis*(2-pyridyl)pyrazine, dpq = (2,3-*bis*(2-pyridyl)quinoxaline, dpb = (2,3-*bis*(2'-pyridyl) benzoquinoxaline, and tpy = 2,2':6',2"-terpyridine.

The visible region of the spectra consists of both Ru ($d\pi$) $\rightarrow$ tpy (π^*) and Ru ($d\pi$) $\rightarrow$ BL (π^*) charge-transfer transitions. The lowest energy electronic absorption bands are the most intense and are assigned Ru $\rightarrow$ BL

CT. For these complexes, the modulation of the energy of the Ru → BL CT transition is dominated by the shift in energy of the BL-based π^* LUMO. In fact, the systematic changes introduced through the series of BLs aids the identification of the Ru → BL CT transitions. The BL-based MLCT's decrease in energy through the series dpp (544 nm), dpq (632 nm), and dpb (682 nm). The red shift in the CT band is due to an increasingly lower-energy BL-based π^* LUMO. For these complexes, the energy of the Ru-based HOMO remains relatively constant as determined by electrochemical analysis. The net result is stepwise lowering of the MLCT depending on BL type.

The monometallic precursors, $[(tpy)RuCl(BL)]^+$, exhibit a similar relationship between MLCT transition wavelength and BL type. For this series, the Ru → BL based MLCT transition wavelengths are reported as 514, 564, and 598 nm for dpp, dpq, and dpb, respectively.[13] Again, a red shift in the MLCT transition is observed as the degree of conjugation of the BL is increased. The transitions for this series of complexes occur at higher energy than for the bimetallic series and indicate the stabilizing effect of $PtCl_2$ coordination on the BL's π^* acceptor orbitals. The BL-dependent changes in energy of the MLCTs substantiate the role of the BL in the lowest energy transition.

The Ru ($d\pi$) → tpy (π^*) CT transition band occurs at approximately 462 nm for the three bimetallic complexes. Absolute assignment of this band is complicated by the presence of other transitions of similar energy. The monometallic precursors exhibit the same Ru → tpy CT transition at similar wavelengths.[13]

Correlation between Spectroscopic and Electrochemical Properties

A correlation can be drawn between the spectroscopic energy gap and the electrochemical energy gap within a series of similar complexes.[43] For the Ru(II)-polypyridyl complexes, the correlation depends on the

assumption that the metal and ligand orbitals involved in the lowest energy MLCT transition are also involved in the metal-based oxidation and first reduction processes. It is expected that the energies of absorption will vary linearly with the differences in redox potentials for the $Ru^{II/III}$ and $BL^{0/-}$ couples [($\Delta E_{1/2} = E_{1/2}$ ($Ru^{II/III}$) - $E_{1/2}$ ($BL^{0/-}$)].[43] Figure 15 is a plot of $\Delta E_{1/2}$ verses E_{abs}(MLCT) for [(tpy)RuCl(BL)](PF_6) and [(tpy)RuCl(BL)$PtCl_2$](PF_6). A

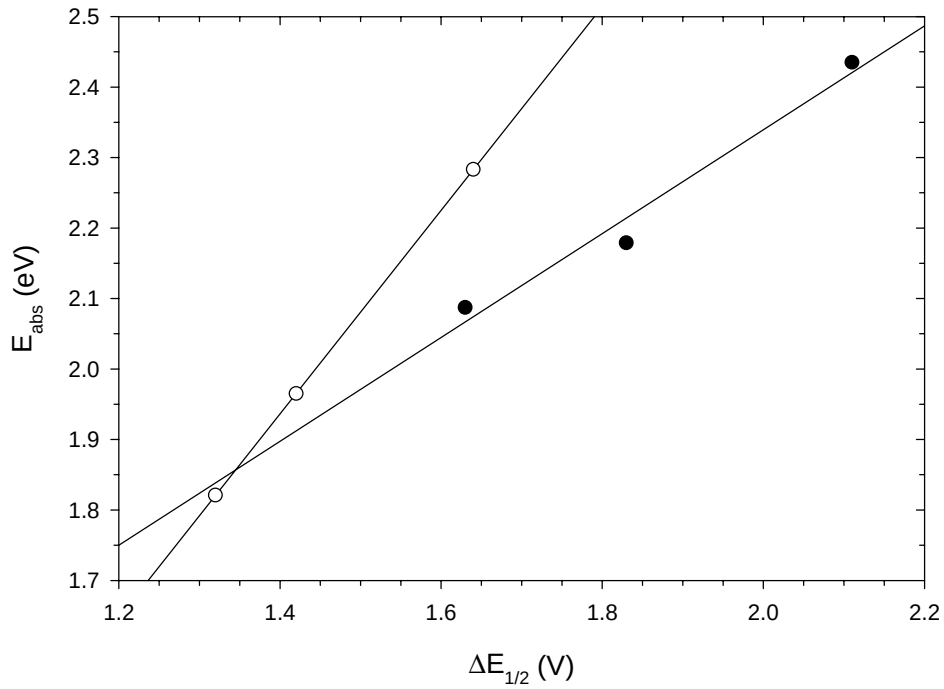

Figure 15. Plot of energies of $E_{1/2}$ (V) vs. the lowest energy absorption band (eV) of $[(tpy)RuCl(BL)]^{1+}$ (●) and $[(tpy)RuCl(BL)PtCl_2]^{1+}$ (○) where BL = dpp, dpq, and dpb.

linear regression analysis has been performed for both sets of data. The Ru-Pt complexes show a linear correlation indicating that the same Ru ($d\pi$) → BL (π^*) CT orbital origin is maintained for the series, $E_{abs} = 1.44\ \Delta E_{1/2} - 0.085$ ($R^2 = 0.999$). Similarly, the monometallic complexes show a linear correlation between the spectroscopic and electrochemical gap, $E_{abs} = 0.737\ \Delta E_{1/2} + 0.865$ ($R^2 = 0.971$). One peculiarity made evident from the analysis is the difference in the slope of the two lines. Due to the similarities in the

two series of complexes, it is expected that the correlation would also display similar slopes with only a change in the y-intercept. This deviation suggests that the coordination of $PtCl_2$ has additional affects on the nature of the BL acceptor orbital and the properties of the complex in general. Additional data points would aid in the interpretation of this plot.

DNA Binding

Agarose gel electrophoresis was used to assess the binding affinity of $[(tpy)RuCl(BL)PtCl_2]^+$ to DNA. When hydrated, agarose forms a matrix that can be cast into gel slabs. Analytes introduced into the matrix can be separated with the application of a voltage across the gel (Figure 16). The mobility of DNA through agarose is dependent on molecular weight, molecular shape, charge, and applied voltage. A change in any of these

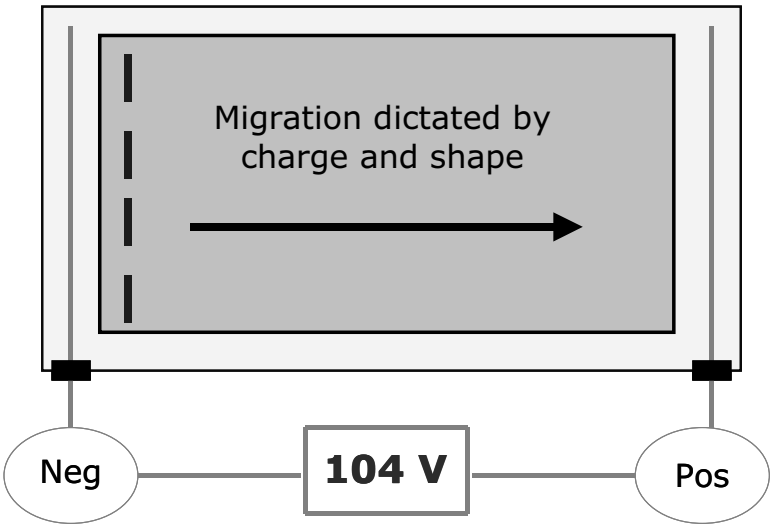

Figure 16. Experimental setup for agarose gel electrophoresis.

factors will affect the rate of migration through the gel. For example, circular plasmid DNA has a supercoiled native state. The same plasmid, with one nick in the sugar-phosphate backbone unwinds and adopts an open circular shape. Supercoiled DNA occupies less volume and therefore migrates through the gel faster than the single-nicked, open circular form.

Figure 17 shows the results of the concentration-dependent DNA-binding study of cisplatin.[32] Each agarose gel contains six lanes. Lane 1 contains a molecular weight standard. Lane 2 contains the plasmid control (2958 bp) with no metal complex added. Lanes 3-6 contain the plasmid DNA incubated for 4 h at 37.8 ^{o}C with varying base pair (bp) to metal complex (mc) ratios; 5:1, 10:1, 20:1, and 100:1. In the absence of cisplatin, the plasmid control migrates inversely proportional to the log of its molecular weight, relative to the MW standard.[32] In lanes 3-6 of each gel, the migration of DNA is hindered substantially. The third lane has the highest relative concentration of metal complex and exhibit the most pronounced effect. In fact, the degree of retardation follows the metal concentration profile with bands having a higher metal concentration being hindered more than bands with lower metal concentrations.

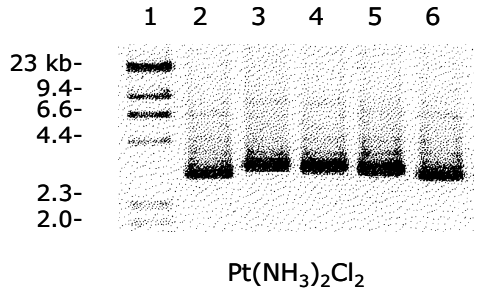

Figure 17. Agarose gel of cisplatin modified DNA (1 = molecular weight std., 2 = linearized pBluescript, 3 = 5 basepairs:1 complex, 4 = 10:1, 5 = 20:1, 6 = 100:1).

Figure 18 shows the results of the concentration-dependent study of the binding of $[(tpy)RuCl(BL)PtCl_2]^+$ complexes to DNA. Again, the concentration of DNA is held constant while the concentration of metal complex is varied. Significant retardation of DNA band migration is observed relative to the migration of the untreated plasmid, similar to that observed for cisplatin. The degree of retardation, however, is greater for the title complexes. These results indicate that the Ru-Pt complex interacts with

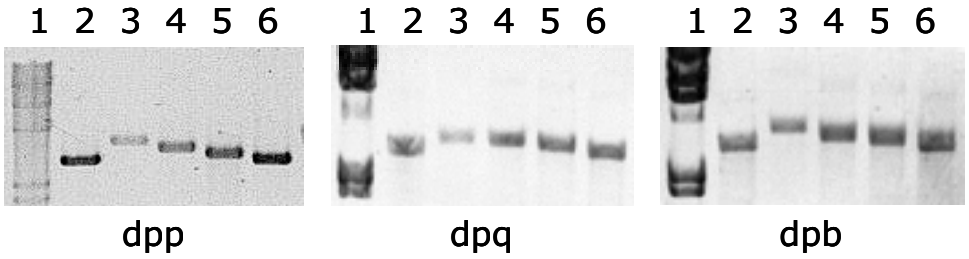

Figure 18. Agarose gels of plasmid DNA incubated with $[(tpy)RuCl(BL)PtCl_2]^+$ where BL = dpp, dpq, and dpb. (1 = molecular weight std., 2 = linearized pBluescript, 3 = 5 basepairs:1 complex, 4 = 10:1, 5 = 20:1, 6 = 100:1).

DNA. The retardation is due to binding of the metal complex to DNA, which both increases the molecular weight and reduces the overall negative charge of the DNA. Because the metal complex must lose one or both platinum-bound chlorides before binding, it will carry a 2^+ or 3^+ charge. When tethered to the anionic plasmid DNA, the overall negative charge of the DNA is reduced and the band migrates at a slower rate. In addition, the bimetallic complexes increase the molecular weight of the DNA fragment, further retarding migration through the gel. The steric demands placed on the plasmid by platinum's coordination sphere should also alter the quaternary structure and affect the migration rate.

The related complexes, $[(bpy)_2Ru(BL)PtCl_2]^{2+}$ and $[(bpy)_2Ru(BL)PtCl_2]^{2+}$, have also been studied with regard to DNA binding affinity.[32] In this study, the two bimetallic complexes are compared to the monometallic precursors $[(bpy)_2Ru(BL)]^{2+}$ and $[(bpy)_2Os(BL)]^{2+}$. The monometallic complexes do not retard the migration of DNA through the gel indicating that no interaction occurs. The two bimetallic complexes do show significant retardation of the DNA. These results indicate that the interaction with DNA is through covalent modification at the $PtCl_2$ site. $[(tpy)RuCl(BL)PtCl_2]^+$ affects the rate of DNA migration similar to these related complexes.

CHAPTER 4: CONCLUSIONS & FUTURE WORK

In this study, a series of complexes of the type $[(tpy)RuCl(BL)PtCl_2](PF_6)$ was synthesized and characterized using FAB-MS, electrochemistry, and electronic absorption spectroscopy. The synthesis follows a building block method where ligands possessing specific properties (i.e. bridging, capping, easily-substituted) and metal atoms are successively added to the supramolecular structure. The general synthetic route allows further modifications of the complex. Using this method, the series $[(tpy)Ru(PEt_2Ph)(BL)PtCl_2]^{2+}$ (PEt_2Ph = diethylphenylphosphine) has since been synthesized by Fang and the spectroscopic and electrochemical properties investigated.[44] The incorporation of the phosphine ligand is designed to offer an additional spectroscopic handle. Due to the number of protons in similar chemical shift environments, the use of ^1H NMR yields little useful information about the structure of the complex. The observation of two ^{31}P chemical shift values for $[(tpy)Ru(PEt_2Ph)(BL)PtCl_2]^{2+}$ by ^{31}P NMR verifies the synthesis of the *cis* and *trans* isomers.[44]

The three title compounds are good light absorbers that exhibited low energy MLCT transitions, which are dependent on the nature of the BL. The energy of these transitions follows the progression seen for the free BLs, dpb < dpq < dpp. It was found that the bimetallic's MLCT transitions occurred at lower energies than the monometallic precursors, indicating the *cis*-$PtCl_2$ coordination has a stabilizing effect on the BL acceptor orbitals.

The trends found in the electronic absorption spectroscopy are consistent with those observed in the electrochemistry. The $BL^{0/-}$ redox couple moves to more positive potentials on going from dpp to dpq to dpb and substantiates the role of BL as the site of location of the LUMO and the acceptor orbital in the MLCT. These $BL^{0/-}$ reduction processes are substantially more cathodic than those observed in $[(tpy)RuCl(BL)]^+$,

indicating coordination of Pt.[32] The second redox process is also BL-based ($BL^{-/2-}$), consistent with the bimetallic formulation of the complexes.[32] Nearly constant potentials were observed for the $Ru^{II/III}$ oxidation couples through out the series, however they occur at slightly more positive potentials than the monometallic precursors. This is due to the electron-withdrawing effect of coordination of electron-deficient Pt^{II}. The presence of the electron-releasing chloride on Ru places the oxidation potential of the $Ru^{II/III}$ redox couple intermediate to that of $[Ru(bpy)_3]^{2+}$ and $Ru(bpy)_2Cl_2$.[4]

This study illustrates the utility of the BL series in tuning the spectroscopic and electrochemical properties of Ru-Pt compexes. In addition, characterization was simplified by allowing the direct comparison of the new complexes. The application of spectroelectrochemistry would lend further evidence to the nature of the electronic absorption spectroscopy. With this technique, changes in the electronic absorption spectroscopy are monitored while the complex is oxidized or reduced. A spectroscopic transition involving orbitals that undergo oxidation or reduction is altered so drastically that the transition is typically no longer seen in the UV-vis region. The oxidation of $Ru^{II/III}$ will blue shift any MLCT involving Ru and red shift the $\pi \rightarrow \pi^*$ intraligand transitions of coordinated ligands. This is due to the increased electron affinity of the higher oxidation state ruthenium. Reductions are isolated in the ligand π^* orbitals. The increase in electron density raises the π^* acceptor orbitals, shifting any transition to this orbital to shorter wavelengths. It is expected that with the oxidation of $[(tpy)RuCl(BL)PtCl_2]^+$, the Ru → BL CT and Ru → tpy CT transitions will move out of the UV-vis region, while the BL and tpy $\pi \rightarrow \pi^*$ transitions will red shift slightly. The reduction of the complex will also move the Ru → BL CT transition out of the UV-vis window. The Ru → tpy CT transition should slightly red shift. These observations would solidify the assignments made for bands appearing in the electronic absorption spectroscopy.

The series has an easily-substituted chloride bound to the light-absorbing Ru chromophore. This sixth coordination site offers further synthetic versatility and another means of tuning the complex's electronic properties. This has previously been shown in the monometallic complexes, $[(tpy)RuCl(BL)]^+$ and $[(tpy)Ru(py)(BL)]^{2+}$.[13] A significantly blue-shifted MLCT transition is observed when substituting py for chloride. The substitution of py also makes the series of complexes luminescent. Similar substutions in the bimetallic complexes $[(tpy)RuCl(BL)PtCl_2]^+$ might lead to luminescent species and would be an interesting extension of the current research.

The three bimetallics show binding to DNA as assessed by agarose gel electrophoresis. As with the model complex, cisplatin, plasmid DNA incubated with the bimetallic complexes migrated slower than untreated plasmid DNA. The migration rate show concentration dependence with higher metal complex-to-DNA base pair ratios running the slowest. Although these results do show metal complex-DNA adduct formation, the efficiency of binding is not known. Studies probing metal complex-DNA binding have been performed for similar complexes using emission-quenching techniques.[45] These studies depend on the attenuation of the emission intensity of $Pt_2(pop)_4^{4-}$ (pop = $P_2O_5H_2^{2-}$) in the presence of a suitable quencher, i.e. $[(tpy)RuCl(BL)PtCl_2]^+$. When DNA is added to a solution of metal complex and $Pt_2(pop)_4^{4-}$ probe, the metal complex binds DNA and is effectively removed from solution. As a result, quenching of the probe's emission is attenuated.[46] The repulsive force between the tetraanionic charge of $Pt_2(pop)_4^{4-}$ and polyanionic charge of DNA hinders any interaction between the two species.[45] This technique has been applied to metals complexes where the affinity is high (10^5 M^{-1}) or low (100 M^{-1}). These experiments would be particularly useful in assessing the efficiency of $[(tpy)RuCl(BL)PtCl_2]^+$-DNA binding.

The mixed-metal complexes form an extension to a class of metal-based systems capable of binding DNA. The modular design allows for component modification to probe the effect of Ru-bound Cl substitution, BL changes, and $PtCl_2$ active site alterations on the DNA-binding, the electronic absorption spectroscopy, and electrochemical characteristics. The modular design also allows for the design of more complicated system incorporating several bioactive sites and additional chromophoric centers. It is possible these systems will be capable of performing intricate functions such a light-activated DNA binding. The new complexes also further the understanding of mixed-metal systems that incorporate the coordinatively unsaturated Pt^{II} moiety.

Appendices

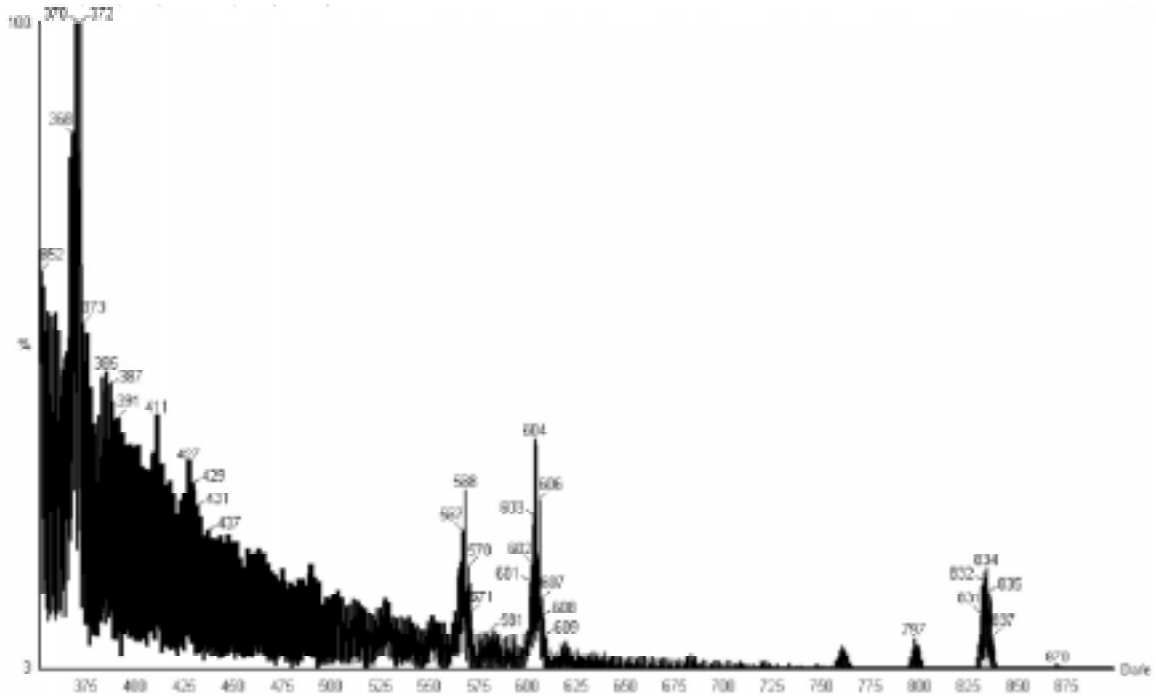

Figure A 1-1. FAB mass spectrum of $[(tpy)RuCl(dpp)PtCl_2](PF_6)$.

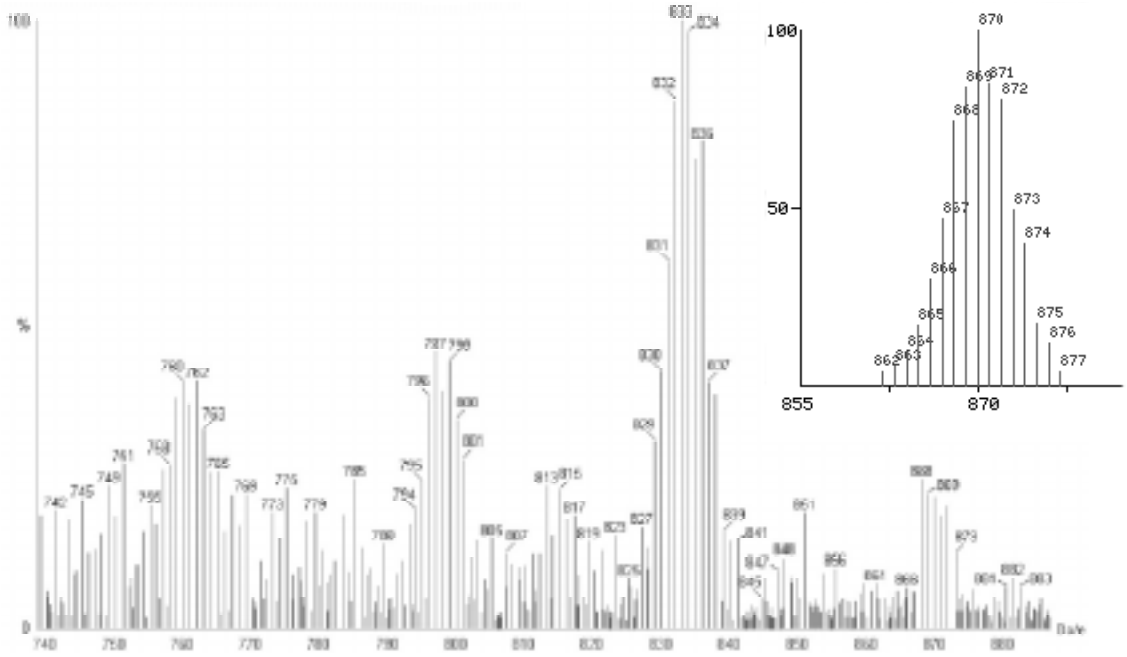

Figure A 1-2. FAB mass Spectrum (high mass range) of [(tpy)RuCl(dpp)$PtCl_2$](PF_6) with calculated isotope pattern (inlay).

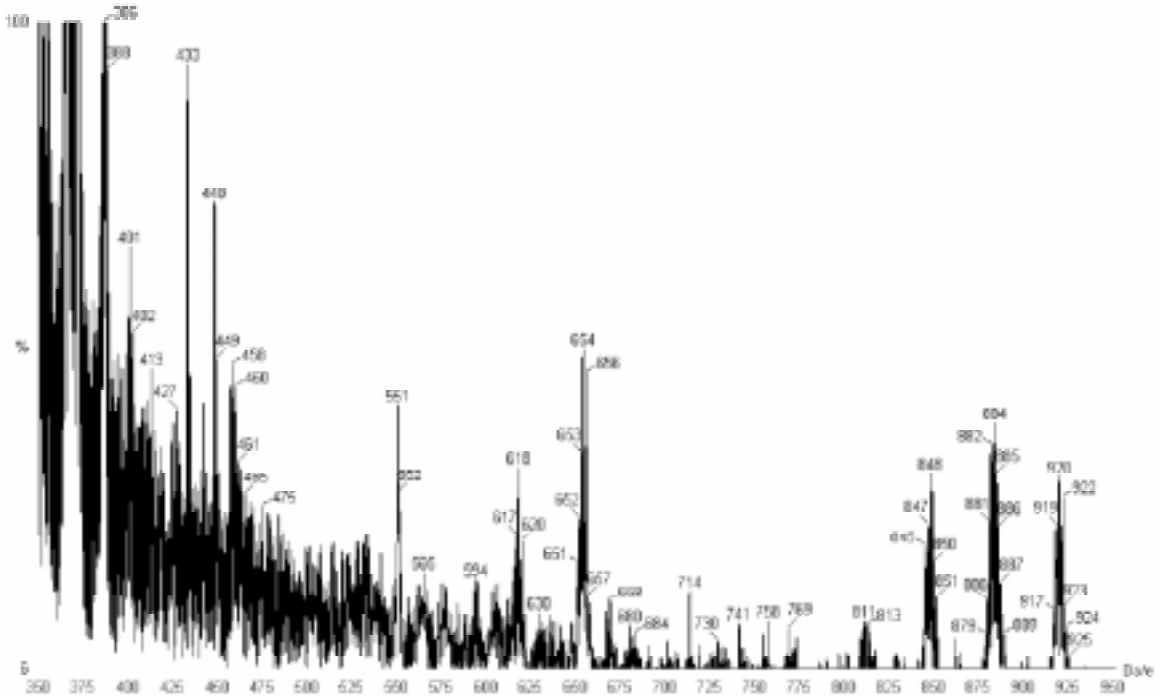

Figure A 2-1. FAB mass spectrum of [(tpy)RuCl(dpq)$PtCl_2$](PF_6).

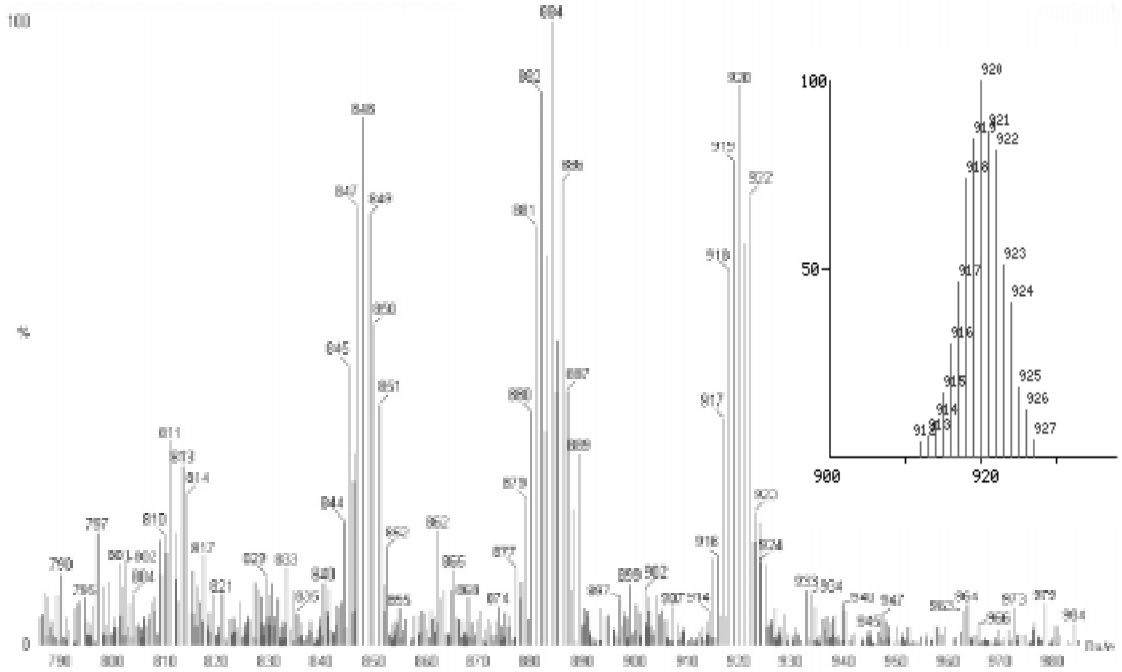

Figure A 2-2. FAB mass Spectrum (high mass range) of [(tpy)RuCl(dpq)$PtCl_2$](PF_6) with calculated isotope pattern (inlay).

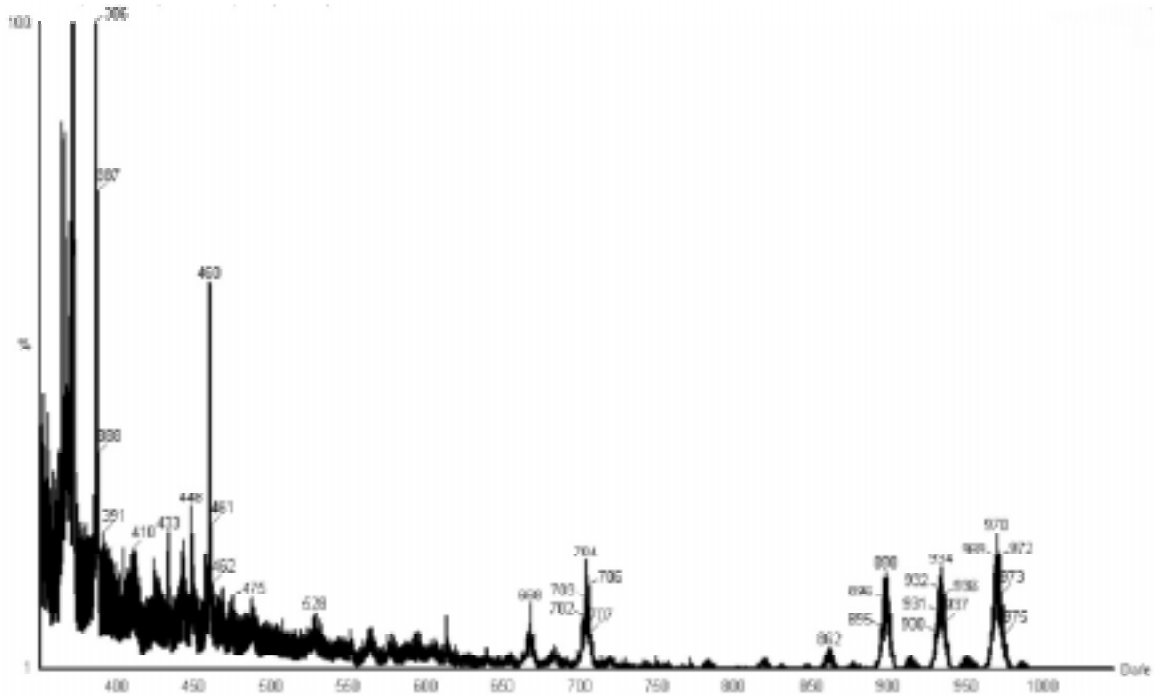

Figure A 3-1 FAB mass spectrum of [(tpy)RuCl(dpb)PtCl$_2$](PF$_6$).

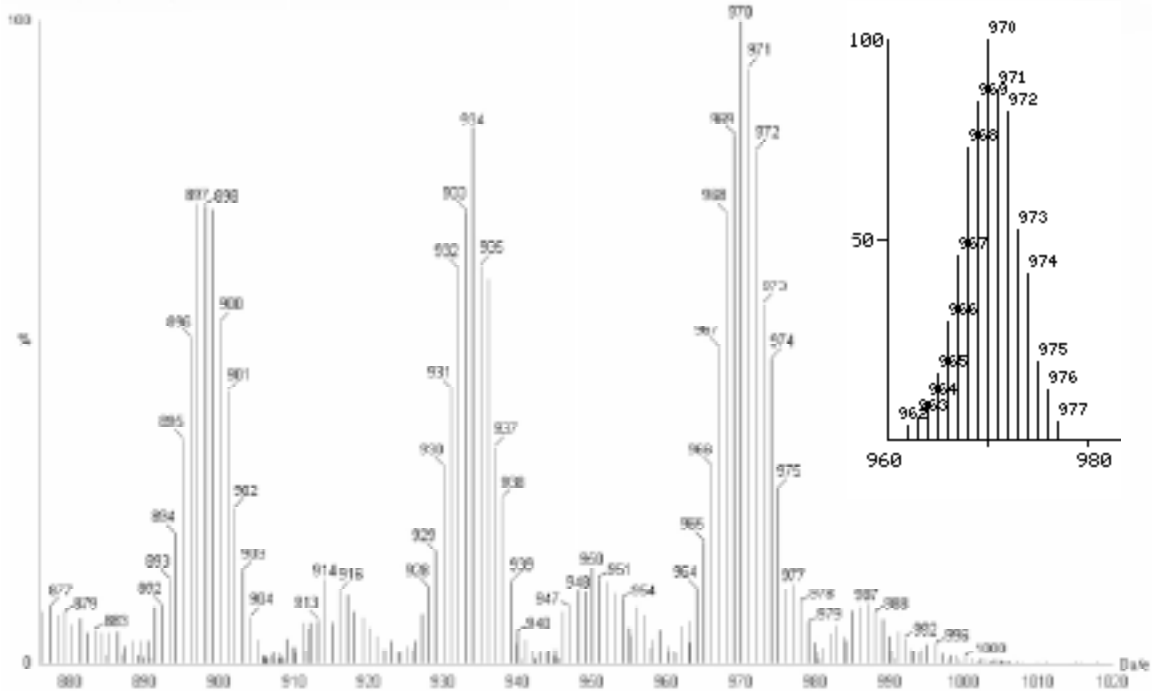

Figure A 3-2. FAB mass Spectrum (high mass range) of [(tpy)RuCl(dpb)$PtCl_2$](PF_6) with calculated isotope pattern (inlay).

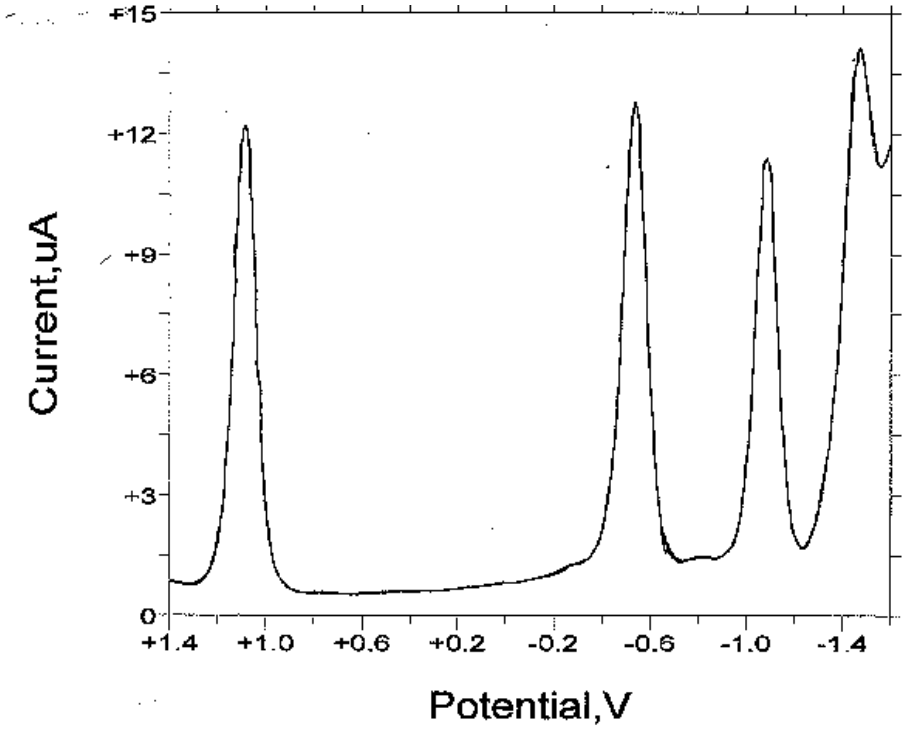

Figure A 4. Square wave voltammogram of [(tpy)RuCl(dpp)PtCl $_2$](PF$_6$).

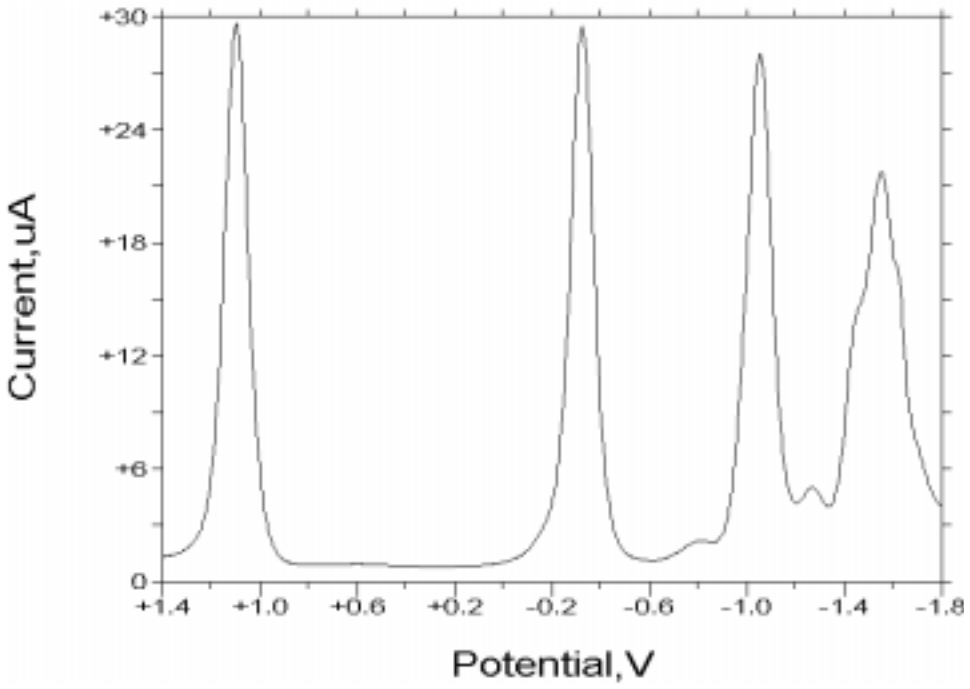

Figure A 5. Square wave voltammogram of [(tpy)RuCl(dpq)PtCl $_2$](PF$_6$).

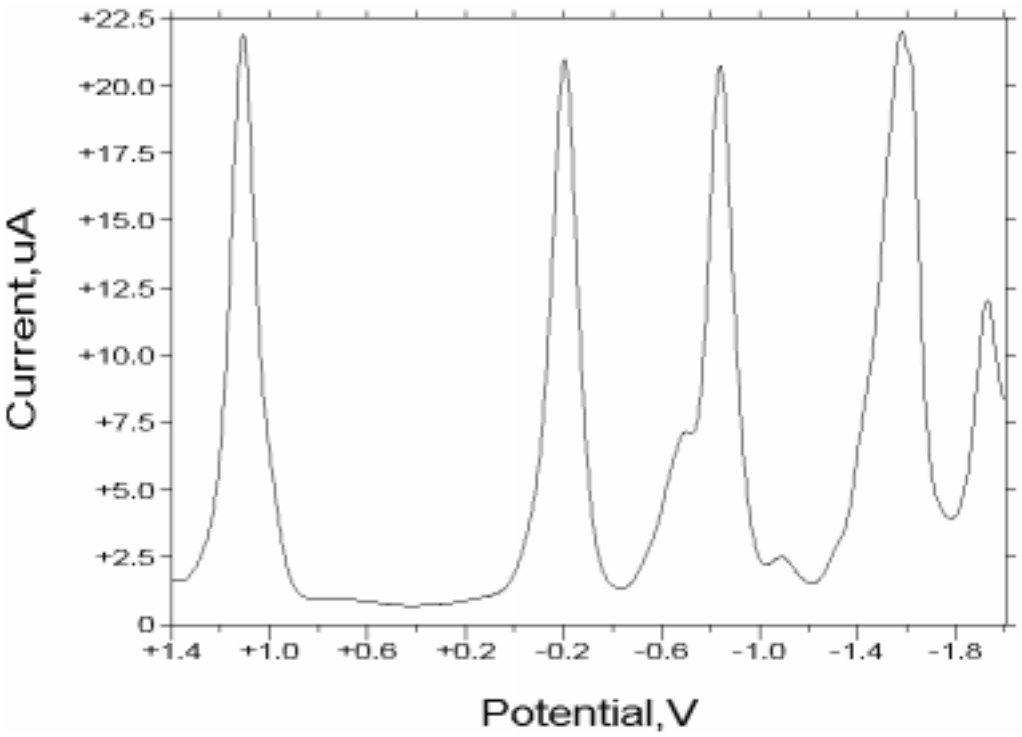

Figure A-6. Square wave voltammogram of [(tpy)RuCl(dpb)PtCl $_2$](PF$_6$).

Bibliography

(1)Kalyanasundaram, K. *Coord. Chem. Rev.* **1982**, *46*, 159-244.
(2)Norris, J.; Meisel, D. *Photochemical energy conversion*; Elsevier: New York, 1989.
(3)Balzani, V.; Scandola, F. J. *Supramolecular Photochemistry*; Horwood: Chichester, U.K., 1991.
(4)KirschDeMesmaeker, A.; Lecomte, J. P.; Kelly, J. M. *Electron Transfer Ii* **1996**, *177*, 25-76.
(5)Belser, P.; Bernhard, S.; Blum, C.; Beyeler, A.; De Cola, L.; Balzani, V. *Coord. Chem. Rev.* **1999**, *192*, 155-169.
(6)Balzani, V.; Juris, A.; Venturi, M.; Campagna, S.; Serroni, S. *Chem. Rev.* **1996**, *96*, 759-833.
(7)Molnar, S. M.; Jensen, G. E.; Vogler, L. M.; Jones, S. W.; Laverman, L.; Bridgewater, J. S.; Richter, M. M.; Brewer, K. J. *J. Photochem. Photobiol. A-Chem.* **1994**, *80*, 315-322.
(8)Marcaccio, M.; Paolucci, F.; Paradisi, C.; Roffia, S.; Fontanesi, C.; Yellowlees, L. J.; Serroni, S.; Campagna, S.; Denti, C.; Balzani, V. *J. Am. Chem. Soc.* **1999**, *121*, 10081-10091.
(9)Meyer, T. J.; Durham, B.; Caspar, V. J.; Nagel, J. K. *J. Am. Chem. Soc.* **1982**, *104*, 4803.
(10)Balzani, V.; Juris, A.; Barigelletti, F.; Belser, P.; Von Zelewsky, A. In *Sci. Pap. Inst. Phys. Chem. Res. (Jpn.)*, 1984; Vol. 78, pp 78-85.
(11)Scandola, F. J.; Roffia, S.; Casadei, R.; Paolucci, F.; Paradisi, C.; Bignozzi, C. *J. Electroanal. Chem.* **1991**, *302*, 157.
(12)Brewer, K. J. *Comments Inorganic Chem.* **1999**, *21*, 201-224.
(13)Vogler, L. M.; Franco, C.; Jones, S. W.; Brewer, K. J. *Inorg. Chim. Acta* **1994**, *221*, 55-59.
(14)Molnar, S. M.; Neville, K. R.; Jensen, G. E.; Brewer, K. J. *Inorg. Chim. Acta* **1993**, *206*, 69-76.
(15)McMillin, D. R.; Hecker, C. R.; Fanwick, P. E. *Inorg. Chem.* **1991**, *30*, 659-666.
(16)Fletcher, N. C.; Keene, F. R. In *J. Chem. Soc., Dalton Trans.*, 1998; pp 2293-2302.
(17)Keene, F. R.; Adcock, P. A. *J. Am. Chem. Soc.* **1981**, *103*, 6494.
(18)Jing, B. W.; Wang, W. Q.; Zhang, M. H.; Shen, T. *Dyes Pigment.* **1998**, *37*, 177-186.
(19)Milkevitch, M.; Shirley, B. W.; Brewer, K. J. *Inorg. Chim. Acta* **1997**, *264*, 249-256.
(20)Wong, E.; Giandomenico, C. M. *Chem. Rev.* **1999**, *99*, 2451-2466.
(21)Saenger, W. *Principles in Nucleic Acid Structure*; Cantor: Springer, Berli, Heidelberg, New York, 1984.

(22)Hoeschele, J. D.; Cleare, M. J. *Bioinorg. Chem.* **1973**, *2*, 187.
(23)Osella, D.; Cavigiolio, G.; Benedetto, L.; Boccaleri, E.; Colangelo, D.; Viano, I. *Inorg. Chim. Acta* **2000**, *305*, 61-68.
(24)Paetz, C.; Paschke, R.; Kalbitz, J. *Inorg. Chim. Acta* **2000**, *304*, 241-249.
(25)Farrell, N.; Bierbach, U.; Qu, Y.; Hambly, T. W.; Peroutka, J.; Nguyen, H. L.; Doedee, M. *Inorg. Chem.* **1999**, *38*, 3535-3542.
(26)Rillema, D. P.; Sahai, R. *Inorg. Chim. Acta* **1986**, *118*, L35-L37.
(27)Rillema, D. P.; Sahai, R.; Baucom, D. A. *Inorg. Chem.* **1986**, *25*, 3843-3845.
(28)Barthram, A. M.; Ward, M. D.; Gessi, A.; Armaroli, N.; Flamigni, L.; Barigelletti, F. *New J. Chem.* **1998**, *22*, 913-917.
(29)Yam, V. W. W.; Lee, V. W. M.; Cheung, K. K. *J. Chem. Soc.-Chem. Commun.* **1994**, 2075-2076.
(30)Yam, V. W. W.; Lee, V. W. M.; Cheung, K. K. *Organometallics* **1997**, *16*, 2833-2841.
(31)Milkevitch, M.; Brauns, E.; Brewer, K. J. *Inorg. Chem.* **1996**, *35*, 1737.
(32)Milkevitch, M.; Storrie, H.; Brauns, E.; Brewer, K. J.; Shirley, B. W. *Inorg. Chem.* **1997**, *36*, 4534-4538.
(33)Kohn, K. W. *Development of Target-Oriented Anticancer Drugs*; Raven Press: New York, 1983.
(34)Zou, Y.; Vanhouten, B.; Farrell, N. *Biochemistry* **1994**, *33*, 5404-5410.
(35)Meyer, T. J.; Sullivan, B. P.; Calvert, J. M. *Inorg. Chem.* **1980**, *19*, 1404.
(36)Wayland, B. B.; Price, J. H.; Williamson, A. N.; Schramm, R. F. *Inorg. Chem.* **1972**, *14*, 1443.
(37)Geiger, W. E.; Connelly, N. G. *Chem. Rev.* **1996**, *96*, 877-910.
(38)Burke, J. F.; Ish-Horowitz, D. *Nucl. Acids. Res.* **1981**, *9*, 2989.
(39)Maniatis, T.; Sambrook, J.; Fritsch, E. F. *Molecular Cloning: A Laboratory Manual*; Cold Spring Harbor Labratory Press: Cold Spring Harbor, NY, 1989, 1989.
(40)Struhl, K.; Ausubel, F.; Brent, R.; Kingston, R. E.; Moore, D. D.; Seidman, J.; Smith, J. A. *Short Protocols in Molecular Biology*; 3rd ed.; Wiley: New York, New York, 1995.
(41)Lions, F.; Goodwin, H. A. *J. Am. Chem. Soc.* **1959**, *81*, 6415.
(42)Gatteschi, D.; Escuer, A.; Comas, T.; Ribas, J.; Vicente, R.; Solans, X.; Zanchini, C. *Inorg. Chim. Acta* **1989**, *162*, 97.
(43)Lever, A. B. P.; Dodsworth, E. S. *Chem. Phys. Lett.* **1985**, *119*, 61-66.
(44)Zhenglai, F. In *The Synthesis and Characterization of a New Kind of Tagged Ru-Pt Bimetallic DNA Binding Agent*; V.P.I. & S.U.: Blacksburg, 2000.
(45)Thorp, H. H.; Carter, R. J.; Ciftan, S. A.; Sistare, M. F. *J. Chem. Ed.* **1997**, *74*, 641-645.

(46)Kalsbeck, W. A.; Thorp, H. H. *J. Am. Chem. Soc.* **1993**, *115*, 7146-7151.

Vita

The author, R. Lee Williams, was born February 4, 1970 in Norfolk, Virginia. After graduating in May of 1988 from Green Run High School in Virginia Beach, Virginia, he pursued an electronics degree while working as an apprentice at the Norfolk Naval Shipyard. After completion of the program, he attended New River Community College in Dublin, Virginia, from August 1991 to May 1992. During this time, he was awarded for his help as a volunteer in the on-campus Tutoring Connection. He attended Virginia Polytechnic Institute and State University from August 1992 to May 1997, graduating with a Bachelor of Science in Chemistry with an emphasis in Biochemistry and a minor in Philosophy. He continued his education in the Virginia Tech graduate program as a Masters student in Inorganic Chemistry under the advisement of Dr. Karen J. Brewer. During this time, he taught General Chemistry, Organic Chemistry, and Inorganic Chemistry. He was honored with the Graduate Teaching Assistant Award in December of 2000. He plans to pursue a Ph.D. in Chemistry at Virginia Tech.